ABSTRACT

VAGHANI, DHWANIL PRAVINBHAI. Liquid Metal Injection Molding: Patterning Liquid Metals for Soft Electronics (Under the direction of Dr. Michael D. Dickey)

Liquid metals are unique elements in the periodic table that possess both the properties of metals and liquids, making them extremely useful as conductors in the advancing field of stretchable electronics. This work studies unique properties possess by alloys of gallium, which are liquid at room temperature (< 30 ^{o}C), possess low viscosity (~2x that of water), density (~6x that of water), high surface tension (720 mN/m, ~10x that of water), low toxicity (relative to mercury) and almost zero vapor pressure. Additionally, it forms a thin (typically ~3nm) passivating native oxide that stabilizes gallium to form non-spherical shapes. The gallium oxide adheres to most of the smooth surfaces which can be useful to pattern liquid metals in several ways that are simply not possible with solid metals.

This work discusses various ways of patterning liquid metals with challenges associated with each of the methods. Following their limitation, we have demonstrated a novel approach to printing liquid metals that is simple, easy, and dependable. Liquid metal injection molding (LMIM) involves the injection of bulk liquid metal through metallophobic microchannel mold to pattern liquid metal geometries in order of sub-microns. The present thesis work follows the process of liquid metal injection molding to pattern various complex geometries with high electrical and mechanical consistency. The method promisingly demonstrates the repetition of printing the liquid metal geometries with the same mold for commercial scale printing of liquid metals.

Subsequently, the present work also demonstrates some exciting applications of the printing method for the making stretchable electrodes, wearable soft heater, soft grippers its use as circuits interconnects, sensors, health monitoring, and soft robots. In addition, we examine the stability of liquid metal patterned wires on different substrates by varying current densities. During this measurement, we found dewetting of LM at a high-temperature point, this gives an important aspect for selective dewetting of bulk liquid metals. Finally, we provide a brief overview of future directions and challenges associated with research involving liquid metals in stretchable electronics.

© Copyright 2022 by Dhwanil Pravinbhai Vaghani

All Rights Reserved

Liquid Metal Injection Molding: Patterning Liquid Metals for Soft Electronics

by

Dhwanil Pravinbhai Vaghani

A thesis submitted to the Graduate Faculty of
North Carolina State University
in partial fulfillment of the
requirements for the degree of
Master of Science

Chemical Engineering

Raleigh, North Carolina
2022

APPROVED BY:

_____	_____
Dr. Saad A Khan	Dr. Jason F Patrick

_____

Dr. Michael D Dickey
Committee Chair

DEDICATION

To my Parents and brother, whose hard work, sacrifice, endless support, and love made this opportunity possible. Thank you for always being there for me.

Nana, thank you for your strength, advice, and love throughout my journey. You are no longer among us, but we remember you every day

BIOGRAPHY

Dhwanil Pravinbhai Vaghani was born on August 31, 1998, in Bhavnagar, Gujarat, India, to Pravinbhai and Bhavnaben Vaghani, and has a younger sibling. He attended Shri H.J Gajera International School in Surat for elementary and middle school before moving on to Gyanmanjri Vidyapith in Bhavnagar for a high school diploma. He then moved to Gandhinagar, Gujarat, to pursue a bachelor's degree in chemical engineering at Pandit Deendayal Energy University (Formerly known as PDPU). He was awarded a third merit medal and merit-cum Scholarship for his excellence in academics. During his undergrad, Dhwanil worked as an undergraduate student researcher at the Office of student outreach program (ORSP) under the supervision of Dr. Manish Kumar Sinha and Dr. Bharti Saini. He has been accoladed with best poster presenter at regional and national conferences. He served as president of the Indian Institute of Chemical Engineers student chapter at PDEU for years (2018-2020).

Dhwanil started as a master's student candidate in the Chemical and Biomolecular Engineering Department at North Carolina State University in Raleigh, NC in Spring'21. He joined Dr. Michael D. Dickey's group as an MS thesis candidate, mentored by Dr. Jinwoo Ma and Dr. Omar Awartani (then post-doctoral candidate and visiting researcher in the Dickey Group). Dhwanil worked as a Graduate Research Assistant on multiple industry-sponsored projects and collaborated with many students in the Dickey Group. Following his graduation, he will be joining GlobalFoundries in Malta, New York as a Process Engineer-Etch.

ACKNOWLEDGMENTS

First and foremost, I would like to thank Dr. Michael D. Dickey for believing in me and giving me the opportunity to work in the group. I consider myself fortunate to have had your unwavering support, generosity, enthusiasm, optimism, and guidance during my master's journey. You are one of the most selfless and kindest people I have ever met and have been a great role model and inspiration to me. I am incredibly grateful for your help in improving my presenting and writing skills. Thank you for your patience as I grew to be a better researcher and person. I would also like to thank Dr. Saad Khan and Dr. Jason Patrick for serving on my thesis committee. Dr. Khan, I am thankful to you for your endless support during the master's program. It has been an honor to be your student.

I would like to extend my sincere regards to Dr. Jinwoo Ma, for helping me to be patient and disciplined with the research. As my mentor, you have always been kind and supportive. We were more than simply coworkers; we were friends who had a great time in the lab carrying out research. I miss our never-ending discussions on culture, language, and food.

I would also want to thank Dr. Omar Awartani for his constant support and direction while working on the "The Aerospace Corporation" project. You are an amazing teacher and mentor. Thank you for showing me how to work efficiently.

A special thanks to everyone in the Dickey group for their continuous help, support, and friendship. It was an honor to be a member of the "work Family," and I couldn't have done it without your support. I would like to thank Minsik Kong, Adam Bachmann, Joe, Milad Shamsi, Sooik Im, Veena Vallem, Meixiang Wang, Tushar Sakorikar, Mansi Patil, Jeongmin Cho, Ethan

Frey, Tamoghna Saha, Sneha Mukherji, Luke Cunningham, Zachary Park, and Sooyoung Kim. You have all taught me so much, and I am grateful for the opportunity to learn from each of you.

I would like to thank all my Raleigh friends who treated me like a family away from home. Shrinivas Katkam, I will always be grateful for your friendship and companionship. Nihar Rao, Jash Diyora, Alekhya Vutukuri, Harshita Koduri, Venkat Sashank, Nandita Raajkumar, Sameera Vellore, Saumil Shah, Bhargav Jethwa, Arth Barot, Rujuta Deo. Thank you for all the wonderful memories.

Finally, I am forever grateful to my parents, whose relentless hard work, endless support, and love made this possible. I am thankful to my younger brother, Jay (thank you for being my support system and for all the motivational conversations).

TABLE OF CONTENTS

LIST OF TABLES

LIST OF FIGURES

CHAPTER 1

INTRODUCTION TO LIQUID METALS

1.1 Introduction

In recent years, liquid metal has gained a lot of attention due to its duality of possessing metallic and fluidic properties intrinsically at or near room temperature. These properties have enabled the use of liquid metals in soft and stretchable electronic devices. Mercury is the most well-known liquid metal; however, its applications are limited due to its toxic nature. Gallium and its alloys, on the other hand, are preferred due to their low toxicity, low melting point, low viscosity, high boiling point, and nearly zero vapor pressure [1]. Other known liquid metals with low melting points such as cesium, rubidium, and francium are not safe for practical applications. Gallium-based liquid metals like eutectic gallium indium (EGaIn), due to their unique ability to resist deformation and retention of electrical conductivity are compelling for applications in soft circuits[2], stretchable wires[3], sensors[4], pumps[5], stretchable antennas[6, 7], and optical structures. [8, 9].

1.2 Gallium alloys

Gallium has piqued curiosity since its discovery in 1875 due to its unique features of combining conductivity and fluidic properties at ambient temperature. Gallium is found on earth as lead, but it is distributed in trace amounts among ores such as bauxite. Thus, the processing required to purify it from other ores, increases its cost despite its overall abundance. Gallium has widely been researched for its use in medical and electronic devices. Studies have been reported for its use as an antimicrobial agent against certain pathogens [10]. However, the wide-scale application of gallium has still not been implemented fully due to the corrosive effects of gallium and its alloys on other metals [11, 12].

1.3 Physical and chemical properties

Gallium is soft, grayish, odorless, and has the lowest melting point of the post-transition metals. The electronic configuration of an element has a significant impact on the melting and boiling point of a metal. Gallium ([Ar] $3d^{10}4s^{2}4p^{1}$) has partially filled p, completely filled s and d shell. The unpaired electrons in the partially filled p shells can form both covalent and metallic bonds. The presence on reactive electrons in the p shell leads to high boiling point (2400 ^{o}C) while the melting point is dependent on the crystal structure of solid phase and degree of delocalization of the valence electrons. Gallium has a melting point of 29 ^{o}C in its purest form, however, this value can decrease when it is alloyed with other metals based on the composition ratio of metals [13]. EGaIn (25% gallium and 75% indium) and Galinstan (68.5 % gallium, 21.5 % indium, 10% tin) have reported melting points around 15.5 ^{o}C and -19 ^{o}C respectively [13].

Table 1: Physical properties of liquid metals, fluids, and conductors

Material	Density	Melting Point (C)	Electrical Resistivity (μΩ .cm)	Thermal Conductivity ($Wm^{-1}. K^{-1}$)
Gallium	5.91	29.8	27.2	30.54
EGaIn	6.25	15.5	29.4	26.43
Galinstan	4.44	10.7	30.3	25.41
DI water	1	0	1.82×10^{13}	0.6
Copper	8.96	1084.6	1.678	401
Silver	10.49	961.8	1.587	429

In addition, gallium and its alloys have the interesting property that, like aluminum, they form a thin oxide layer (~3nm) on its surface when exposed to oxygen at ambient temperature[14].

Normally, liquids with low viscosity and high surface tensions tends to bead up spherically on the surface to minimize the surface energy. Yet, the oxide allows gallium to maintain non-spherical shapes. In the absence of oxide, small volume of Ga will bead up spherically. The oxide skin is amphoteric and can be removed by strong acid or base (NaOH/ HCl) at pH < 3 or pH > 10 [15].

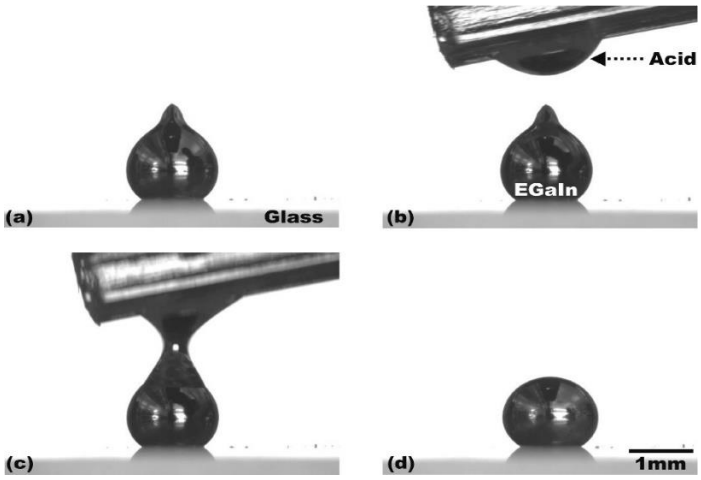

Figure 1: (a, b) Gallium alloys can gain a non-spherical shape due to presence of thin native oxide, and (c, d) Exposure to acid/base oxide get dissolve causing the metal to bead up due to high surface tension [15]

The intrinsic properties of gallium based liquid metal to form a thin native oxide has limited its application in several ways. The adhesive nature of these oxide enables them to get adhere to many surfaces which inhibits the flow property, making it difficult to be used for fluidic applications. Gallium and its alloys leave metal oxide on most surfaces, posing handling issues in the laboratory and in a manufacturing environment. The oxide also forms a thin barrier layer that eliminates the physical contact of metal with the surroundings. It also interferes with the electrochemical properties, which also limits the use of gallium. Therefore, despite being toxic, mercury has been used for its application in thermometers, barometers, dental amalgams, polygraphy, micropumps, valves, and optical switches [16-17]. However, oxide plays a pivotal role in the mechanical stability of the gallium. The oxide that forms on gallium alloys possess yield stress of ~0.4 – 0.6 N/m and below the critical yield stress, the oxide skin is elastic and stable at ambient

temperature but beyond that, the oxide layer splits and the low viscosity metals flow smoothly on the substrate[15]. As a result, it is feasible to pattern liquid metal into different geometries that are difficult to do with other conventional liquids. The ability of LM to flow by breaking oxide beyond critical stress and rapidly reforming of oxide for stress lower than the critical stress, has opened the ways to pattern liquid metals for use in soft and stretchable electronics.

1.4 Liquid metal patterning

Liquid metal pattering is a topic of interest as they enable optical and electrical component in the circuits that are soft, stretchable, and deformable. The thin elastic oxide formed around the metal upon its exposure to oxygen have significantly impacted its rheological behavior and adhesion on substrates[15]. Liquid metal encased in elastomer can be deformed elastically to large strains while maintaining excellent electrical conductivity. This electromechanical response makes it desirable for stretchable conductors and composites. Unlike conventional metals, liquid metal can be injected into microfluidic channels or can be direct written on various substrates which makes it an inexpensive, easy, and fast way of fabricating electronic devices [27]. Liquid metals can be patterned on a variety of substrates including gels, polymer, elastomers, biological materials and fabric at ambient temperature and pressure. Liquid metal can be patterned without the need of high-cost processing including vacuum deposition, physical vapor deposition and sputtering that are used conventionally for the deposition of solid metals. Moreover, the fluidic property of liquid metal allows for the fabrication of shape reconfigurable devices.

Gallium-based alloys possess intrinsic property of forming a native thin oxide that has enabled their micro-scale patterning at room temperature. Previous studies have demonstrated various patterning techniques for patterning liquid metals with each having its own merits and demerits [27]. The application of these patterning techniques has resulted in varying feature size of

the geometries. This section briefly discusses different patterning techniques to highlight their capabilities, limitations, and scope of improvements for advancement in the field.

1.4.1 Imprinting

Previous work has reported an interesting way of imprint lithography-based pattering of liquid metal on elastomeric substrates for its application in making stretchable interconnects[18].

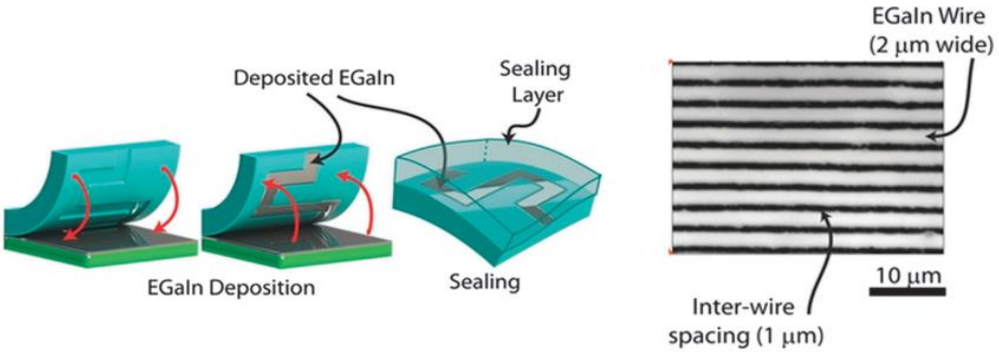

Figure 2: Imprint lithography for patterning of liquid metal

Imprinting liquid metal with elastomeric molds involves spreading the liquid metal film uniformly on the planar substrate onto which elastomeric mold with fine topographical feature is pressed. The oxide adheres to the cavities of the mold and this causes metal to remain stuck in the feature even after lifting the mold off from the substrate. The mold with the EGaIn filled cavities is then encapsulated by another layer of elastomer for its use in stretchable electronic devices. The method demonstrated to pattern geometries having dimensions of 2 μm width and submicron depth.

1.4.2 Selective adhesion

The interfacial properties of substrate and liquid metal reflects the wetting and non-wetting behavior of liquid metals on the substrate. Liquid metal with the native oxide layer adheres to most of the smooth surfaces while it has poor adherence with the rough surfaces. Such rough surfaces are termed as metallophobic surfaces [19, 20]. The substrate properties can be altered to enable

selective wetting of metals [21, 22]. Spreading the metal uniformly on the pre-modified substrate with wetting and non-wetting region offers a novel way to pattern the metal.

1.4.3 Stencil printing

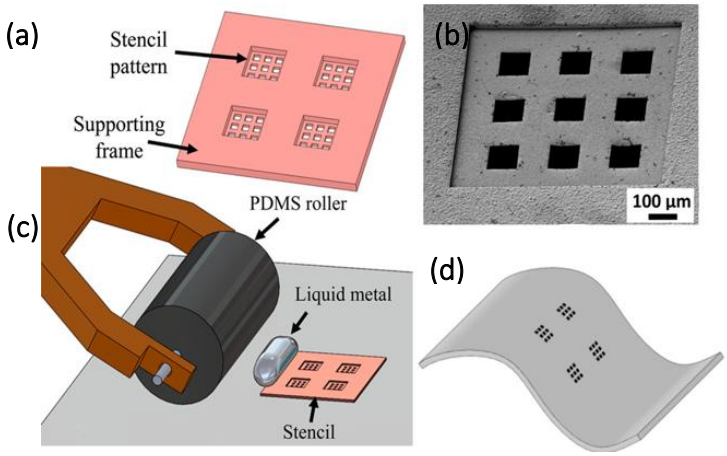

Figure 3: Thin stencils can increase the resolution of LM designs. A thin 3 mm metal stencil backed by a thicker frame layer yielded 10 µm LM features [23]

Stencil printing of liquid metal is a high throughput method of patterning liquid metals that uses stiff stencils to pattern desired geometries on various substrates[24]. As shown in Figures 3(a, b) a stencil pattern is crafted on a supporting frame. Liquid metal is spread uniformly across the stencil using a hand roller as shown in Figure 3(c). Liquid metal with oxides will get adhered to the surface. The stencils are then peeled off leaving LM patterns on the substrate with fine geometries of 10 µm in width. The feature size of the patterned geometries highly depends upon the preparation of stencils [23].

1.4.4 Direct writing

The unique property of gallium-based LM of forming a stable oxide layer on the surface enables different ways of direct writing of LM [25]. Typically, the direct writing method involves the extrusion of LM through a syringe tip using a pneumatic or liquid displacement pump. The method relies heavily on adhesion between the substrate and LM oxide, weak adhesion between

them results in an unfavorable pattern. LM drops can be stacked to a height of 1 cm, enabling 3D patterns[25]. The interfacial characteristics of the substrate can be changed to improve the adherence of oxide to the surface. For printing the LM in a controlled fashion, the nozzle diameter, rate of LM extrusion, dispensing pressure, and height between the substrate and nozzle tip are all essential parameters[26]. The direct writing of LM works well on smooth and hydrophilic surfaces however, it gets challenging with rough surfaces where there is poor contact between the oxide and substrate.

1.4.5 Injection

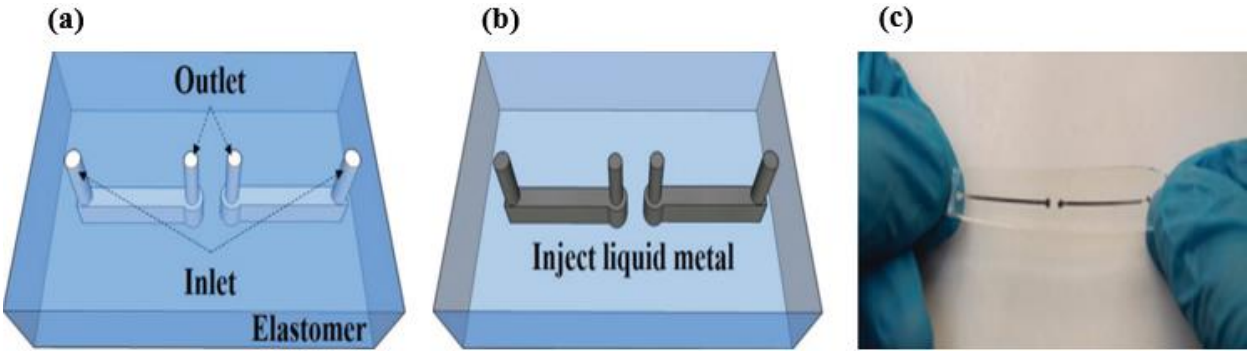

Figure 4: (a) Microfluidic channels within elastomer formed by replica molding. (b) The liquid metal is filled in the microchannel using a syringe (c) Flexible dipole antenna made by injection of liquid metal inside the elastomer[27].

The injection of LM through microfluidic channels has been utilized widely in soft matter electronics applications. The methods involve injecting LM through prefabricated microfluidic channels with inlet and outlet holes using nozzles. The thin oxide formed by LM helps in maintaining a stable non-spherical geometry. The injection of LM into microfluidic channels necessitates a significant differential pressure to break the oxide and displace the air in the channel, allowing the LM to flow. The LM forms a stable oxide at all interfaces after injection, resulting in continuous stable geometry. The holes at the two ends of the channel are then sealed with silicones or elastomers to prevent leakage. In some cases, the oxide adheres to the smooth channels. Injecting a carrier fluid before injecting the LM introduces a slip layer between the oxide and wall of channels. This enables reversible actuation of LM within microfluidic channels [28].

1.5 Vacuum filling

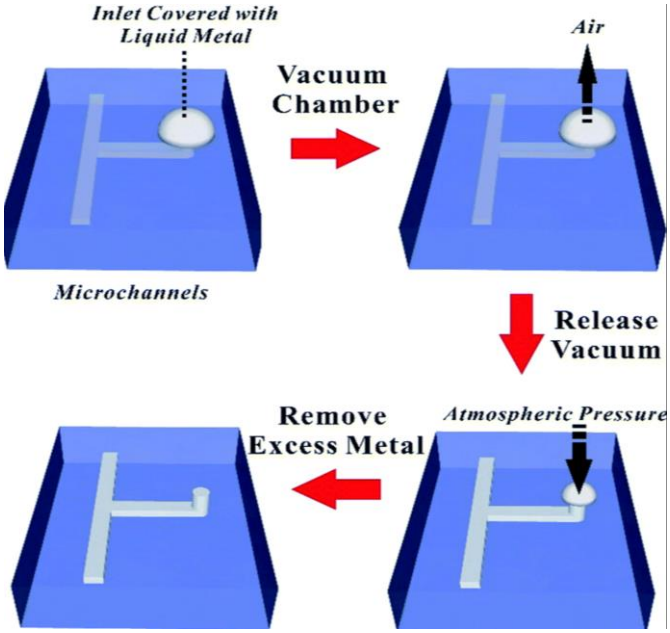

Figure 5: Process schematic of vacuum filling of liquid metals into a microfluidic channel. This involves a mold with an inlet hole covered with the LM droplet. The entire substrate is placed in a vacuum chamber where air bubbles from droplet as well as the substrate are removed and liquid metal fills the microchannels [29].

Vacuum filling resembles the injection method where a prefabricated microfluidic channel is used to cast the pattern on the substrate. The process includes a slug of LM placed on the inlet hole of the microfluidic channel. The entire setup is then placed in a vacuum where the LM displaces the air out of the channel to form fine featured geometry with dimensions as small as 5-10 µm [30]. Vacuum filling is used generally for the patterning of complex shapes or geometries as there is always a risk of leakage in case of manual filling of the microfluidic channels[31]. Although the technology has a potential for patterning complicated designs, the entire process takes longer than previously mentioned methods. It requires a continuous pathway for LM to flow is required and any blockage can result in discontinuous patterns. Hence, the vacuum filling method is used selectively based upon the complexities and application of the pattern.

1.6 Applications

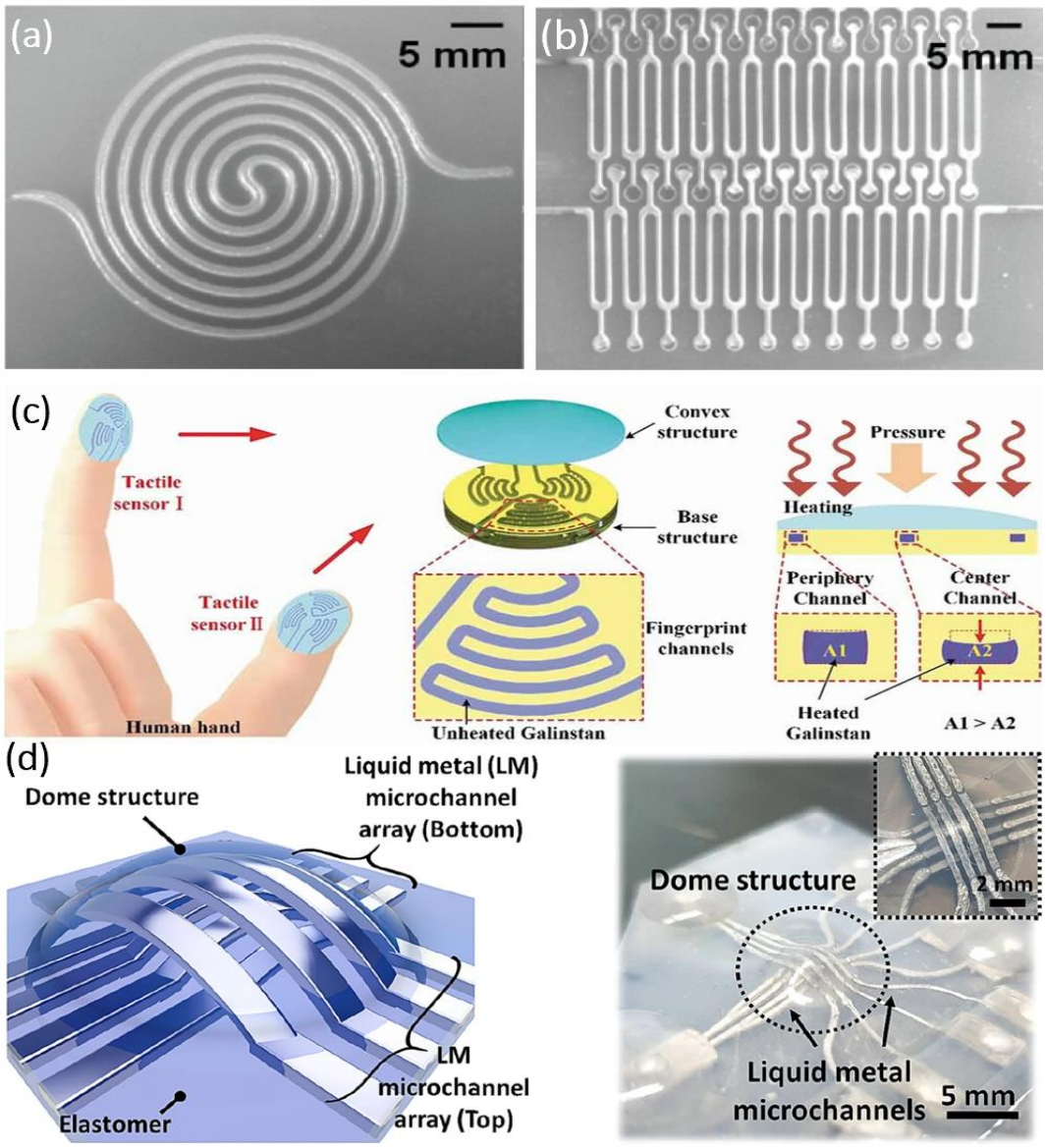

Figure 6: Pressure sensing using (a) Spiral shape and (b) serpentine-shaped EGaIn microchannel encapsulated in silicone (elastomer) caused by changes in electrical conductivity with regard to changes in dimensions for the geometry [32](c) Flexible tactile sensors with fingerprint patterned microfluidic channels embedded with Galinstan to measure the temperature and contact force[33] (d) LM-Based multiaxial flexible force sensors for electronic skin [34].

The ability to print liquid metals on a wide range of substrates with small to large feature sizes depending on the application has made its way for its use in wearable electronics. Figure 6(a) and 6(b) reports spiral and serpentine microchannels filled with EGaIn and encapsulated with silicone. The primary objective was to use external deformative forces to alter the dimension of

the LM geometries to harness the change in electrical resistance for sensing. The basic principle here is the change that enable the increase or decrease of the resistance value when external axial or tangential forces cause physical deformation. This sensing therefore can be utilized in many soft or flexible actuator applications. Figure 6(c) reports the fabrication of a soft tactile sensor for force and temperature sensing applications. A digital light processing printing was used to make fingerprint shape microfluidic channels on the elastomer to sense the force applied to it along with the temperature. The fabricated sensor is reported to possess a relatively high sensing ability of 0.29 N^{-1} and 0.55% at 20 to 50 ^{o}C. It also possesses relatively high durability and flexibility that can potentially be used in various application such as soft robotics[35- 36], smart prosthetics [37-39] and medical health monitoring devices [40]. Figure 6(d) manifests the fabrication of a soft multi-axial force sensor for the e-skin application. It indulges two distinct layers of microfluidic channels embedded with LM that are positioned on top of one another. The force was applied with a finger to cause physical deformation which mechanically alters its electrical resistance, and the response was measured; the sensor was mentioned to be relatively highly durable and stretchable.

1.7 Outline of thesis

Chapter 1 gives an overview of liquid metals and how they are classified based on their physical and chemical properties. It also provides a brief overview of various patterning techniques for patterning liquid metal on various substrates. Finally, it also highlights some interesting applications of printed bulk liquid metal in the field of soft electronics.

Chapter 2 proposes a novel method of patterning Liquid metal that is simple, dependable, and highly consistent. The method is very similar to traditional injection molding of solid conventional metals. This chapter concentrates on the stages involved in injection molding of liquid metal and efforts to optimize various parameters to enable consistent printing of LM.

Chapter 3 focuses on harnessing the injection patterning method for two applications: stretchable heaters for use in thermotherapy, and electroadhesive in soft actuators.

Chapter 4 will provide brief concluding notes for the thesis, discussing future research directions and potential commercialization applications for the soft electrical devices presented in Chapter 3.

1.8 References

(1) Dickey, M. D. Stretchable and Soft Electronics Using Liquid Metals. *Adv. Mater.* **2017**, *29* (27), 1606425. https://doi.org/10.1002/adma.201606425.

(2) Lin, Y.; Cooper, C.; Wang, M.; Adams, J. J.; Genzer, J.; Dickey, M. D. Handwritten, Soft Circuit Boards and Antennas Using Liquid Metal Nanoparticles. *Small* **2015**, *11* (48), 6397–6403. https://doi.org/10.1002/smll.201502692.

(3) *Self-Healing Stretchable Wires for Reconfigurable Circuit Wiring and 3D Microfluidics - Palleau - 2013 - Advanced Materials - Wiley Online Library*. https://onlinelibrary.wiley.com/doi/abs/10.1002/adma.201203921 (accessed 2022-08-07).

(4) Majidi, C.; Kramer, R.; Wood, R. J. A Non-Differential Elastomer Curvature Sensor for Softer-than-Skin Electronics. *Smart Mater. Struct.* **2011**, *20* (10), 105017. https://doi.org/10.1088/0964-1726/20/10/105017.

(5) *Liquid metal enabled pump | PNAS*. https://www.pnas.org/doi/abs/10.1073/pnas.1319878111 (accessed 2022-08-07).

(6) Markvicka, E. J.; Bartlett, M. D.; Huang, X.; Majidi, C. An Autonomously Electrically Self-Healing Liquid Metal-Elastomer Composite for Robust Soft-Matter Robotics and Electronics. *Nat. Mater.* **2018**, *17* (7), 618–624. https://doi.org/10.1038/s41563-018-0084-7.

(7) *Reversibly Deformable and Mechanically Tunable Fluidic Antennas - So - 2009 - Advanced Functional Materials - Wiley Online Library*. https://onlinelibrary.wiley.com/doi/pdf/10.1002/adfm.200900604 (accessed 2022-08-07).

(8) Park, C. W.; Moon, Y. G.; Seong, H.; Jung, S. W.; Oh, J.-Y.; Na, B. S.; Park, N.-M.; Lee, S. S.; Im, S. G.; Koo, J. B. Photolithography-Based Patterning of Liquid Metal Interconnects for Monolithically Integrated Stretchable Circuits. *ACS Appl. Mater. Interfaces* **2016**, *8* (24), 15459–15465. https://doi.org/10.1021/acsami.6b01896.

(9) Chen, T.; Dai, L. Carbon Nanomaterials for High-Performance Supercapacitors.Mater. *Today* **2013**.

(10) Chitambar, C. R. Medical Applications and Toxicities of Gallium Compounds. *Int. J. Environ. Res. Public. Health* **2010**, *7* (5), 2337–2361. https://doi.org/10.3390/ijerph7052337.

(11) Deng, Y.-G.; Liu, J. Corrosion Development between Liquid Gallium and Four Typical Metal Substrates Used in Chip Cooling Device. *Appl. Phys. A* **2009**, *95* (3), 907–915. https://doi.org/10.1007/s00339-009-5098-1.

(12) Cui, Y.; Ding, Y.; Xu, S.; Yang, Z.; Zhang, P.; Rao, W.; Liu, J. Liquid Metal Corrosion Effects on Conventional Metallic Alloys Exposed to Eutectic Gallium–Indium Alloy Under Various Temperature States. *Int. J. Thermophys.* **2018**, *39* (10), 113. https://doi.org/10.1007/s10765-018-2440-x.

(13) Daeneke, T.; Khoshmanesh, K.; Mahmood, N.; Castro, I. A. de; Esrafilzadeh, D.; Barrow, S. J.; Dickey, M. D.; Kalantar-zadeh, K. Liquid Metals: Fundamentals and Applications in

Chemistry. *Chem. Soc. Rev.* **2018**, *47* (11), 4073–4111. https://doi.org/10.1039/C7CS00043J.
(14) *Eutectic Gallium-Indium (EGaIn): A Liquid Metal Alloy for the Formation of Stable Structures in Microchannels at Room Temperature - Dickey - 2008 - Advanced Functional Materials - Wiley Online Library*. https://onlinelibrary.wiley.com/doi/10.1002/adfm.200701216 (accessed 2022-08-08).
(15) *Emerging Applications of Liquid Metals Featuring Surface Oxide | ACS Applied Materials & Interfaces*. https://pubs.acs.org/doi/10.1021/am5043017 (accessed 2022-08-08).
(16) Yun, K.-S.; Cho, I.-J.; Bu, J.-U.; Kim, C.-J.; Yoon, E. A Surface-Tension Driven Micropump for Low-Voltage and Low-Power Operations. *J. Microelectromechanical Syst.* **2002**, *11* (5), 454–461. https://doi.org/10.1109/JMEMS.2002.803286.
(17) Shen, W.; Edwards, R. T.; Kim, C.-J. Electrostatically Actuated Metal-Droplet Microswitches Integrated on CMOS Chip. *J. Microelectromechanical Syst.* **2006**, *15* (4), 879–889. https://doi.org/10.1109/JMEMS.2006.878877.
(18) *High-Density Soft-Matter Electronics with Micron-Scale Line Width - Gozen - 2014 - Advanced Materials - Wiley Online Library*. https://onlinelibrary.wiley.com/doi/abs/10.1002/adma.201400502 (accessed 2022-08-08).
(19) Kramer, R. K.; Boley, J. W.; Stone, H. A.; Weaver, J. C.; Wood, R. J. Effect of Microtextured Surface Topography on the Wetting Behavior of Eutectic Gallium-Indium Alloys. *Langmuir ACS J. Surf. Colloids* **2014**, *30* (2), 533–539. https://doi.org/10.1021/la404356r.
(20) Kim, D.; Jung, D.; Yoo, J. H.; Lee, Y.; Choi, W.; Lee, G. S.; Yoo, K.; Lee, J.-B. Stretchable and Bendable Carbon Nanotube on PDMS Super-Lyophobic Sheet for Liquid Metal Manipulation. *J. Micromechanics Microengineering* **2014**, *24* (5), 055018. https://doi.org/10.1088/0960-1317/24/5/055018.
(21) Kim, H.-J.; Son, C.; Ziaie, B. A Multiaxial Stretchable Interconnect Using Liquid-Alloy-Filled Elastomeric Microchannels. *Appl. Phys. Lett.* **2008**, *92* (1), 011904. https://doi.org/10.1063/1.2829595.
(22) Kramer, R. K.; Majidi, C.; Wood, R. J. Masked Deposition of Gallium-Indium Alloys for Liquid-Embedded Elastomer Conductors. *Adv. Funct. Mater.* **2013**, *23* (42), 5292–5296. https://doi.org/10.1002/adfm.201203589.
(23) Lazarus, N.; Bedair, S. S.; Kierzewski, I. M. Ultrafine Pitch Stencil Printing of Liquid Metal Alloys. *ACS Appl. Mater. Interfaces* **2017**, *9* (2), 1178–1182. https://doi.org/10.1021/acsami.6b13088.
(24) Jeong, S. H.; Hagman, A.; Hjort, K.; Jobs, M.; Sundqvist, J.; Wu, Z. Liquid Alloy Printing of Microfluidic Stretchable Electronics. *Lab. Chip* **2012**, *12* (22), 4657–4664. https://doi.org/10.1039/C2LC40628D.
(25) Ladd, C.; So, J.-H.; Muth, J.; Dickey, M. D. 3D Printing of Free-Standing Liquid Metal Microstructures. *Adv. Mater.* **2013**, *25* (36), 5081–5085. https://doi.org/10.1002/adma.201301400.

(26) Lu, T.; Finkenauer, L.; Wissman, J.; Majidi, C. Rapid Prototyping for Soft-Matter Electronics. *Adv. Funct. Mater.* **2014**, *24* (22), 3351–3356. https://doi.org/10.1002/adfm.201303732.
(27) Joshipura, I. D.; Ayers, H. R.; Majidi, C.; Dickey, M. D. Methods to Pattern Liquid Metals. *J. Mater. Chem. C* **2015**, *3* (16), 3834–3841. https://doi.org/10.1039/C5TC00330J.
(28) Khan, M. R.; Trlica, C.; So, J.-H.; Valeri, M.; Dickey, M. D. Influence of Water on the Interfacial Behavior of Gallium Liquid Metal Alloys. *ACS Appl. Mater. Interfaces* **2014**, *6* (24), 22467–22473. https://doi.org/10.1021/am506496u.
(29) Lin, Y.; Gordon, O.; Khan, M. R.; Vasquez, N.; Genzer, J.; Dickey, M. D. Vacuum Filling of Complex Microchannels with Liquid Metal. *Lab. Chip* **2017**, *17* (18), 3043–3050. https://doi.org/10.1039/C7LC00426E.
(30) *3D structures of liquid-phase GaIn alloy embedded in PDMS with freeze casting - Lab on a Chip (RSC Publishing) DOI:10.1039/C3LC50833A*. https://pubs.rsc.org/en/content/articlehtml/2013/lc/c3lc50833a?casa_token=TzGV4uMU3qsAAAAA:UUc9mKG9wTsGLyg8F9uvXMVvk9bl0uB9LSONBO63g1W0w6_tlWmpLT-f5_4lPkqgYeMLvWeCb2CtHg (accessed 2022-08-13).
(31) Wang, X.; Ma, Y.; Xue, Y.; Luan, H.; Pharr, M.; Feng, X.; Rogers, J. A.; Huang, Y. Collapse of Liquid-Overfilled Strain-Isolation Substrates in Wearable Electronics. *Int. J. Solids Struct.* **2017**, *117*, 137–142. https://doi.org/10.1016/j.ijsolstr.2017.03.031.
(32) Krause, A. Hyperelastic Pressure Sensing with a Liquid Embedded Elastomer. *The Robotics Institute Carnegie Mellon University*.
(33) *Full article: 3D Printing of Liquid Metal Based Tactile Sensor for Simultaneously Sensing of Temperature and Forces*. https://www.tandfonline.com/doi/full/10.1080/19475411.2021.1948457 (accessed 2022-08-09).
(34) Kim, K.; Ahn, J.; Jeong, Y.; Choi, J.; Gul, O.; Park, I. All-Soft Multiaxial Force Sensor Based on Liquid Metal for Electronic Skin. *Micro Nano Syst. Lett.* **2021**, *9* (1), 2. https://doi.org/10.1186/s40486-020-00126-9.
(35) Carrico, J. D.; Tyler, T.; Leang, K. K. A Comprehensive Review of Select Smart Polymeric and Gel Actuators for Soft Mechatronics and Robotics Applications: Fundamentals, Freeform Fabrication, and Motion Control. *Int. J. Smart Nano Mater.* **2017**, *8* (4), 144–213. https://doi.org/10.1080/19475411.2018.1438534.
(36) Luo, S.; Bimbo, J.; Dahiya, R.; Liu, H. Robotic Tactile Perception of Object Properties: A Review. arXiv November 10, 2017.
(37) Abd, M.; Paul, R.; Aravelli, A.; Bai, O.; Lagos, L.; Lin, M.; Engeberg, E. Hierarchical Tactile Sensation Integration from Prosthetic Fingertips Enables Multi-Texture Surface Recognition. *Sensors* **2021**, *21*, 29. https://doi.org/10.3390/s21134324.
(38) Fishel, J.; Loeb, G. Bayesian Exploration for Intelligent Identification of Textures. *Front. Neurorobotics* **2012**, *6*.

(39) Lu, T.; Markvicka, E. J.; Jin, Y.; Majidi, C. Soft-Matter Printed Circuit Board with UV Laser Micropatterning. *ACS Appl. Mater. Interfaces* **2017**, *9* (26), 22055–22062. https://doi.org/10.1021/acsami.7b05522.

CHAPTER 2

LIQUID METAL INJECTION MOLDING

2.1 Introduction

The combined fluidic and conductive properties of liquid gallium (and its alloys) have led to new ways to fabricate soft and stretchable electronics. The ability to maintain its functionality upon mechanical deformation has enabled its use in wearable electronics, sensors, medical implants [2], capacitive sensors [3], prosthetics [4,5], and soft robotic actuations[6]. Patterning of LM has therefore become a very crucial step for fabricating soft electronic devices for various applications. Injection of liquid metals into microfluidic channels[7–11], appears to be a very viable option for patterning since it is relatively simple, reproducible, and consistent. Despite its simplicity, the methods hold certain drawbacks which limit its application. The prefabricated microchannel molds used for the injection of microchannels are often made using lithographic tools which increase the cost and time of the patterning process [12,13]. The microchannel molds are difficult to combine with the external circuit components. There is always a risk of microchannels collapsing in the mold. This challenge can be addressed with direct writing of liquid metal [14], but it can only be used to the pattern on the flat substrates. In addition, it uses a complex mechanical system[15]. To overcome these difficulties, a novel method is introduced for easy, reliable, and consistent patterning of liquid metal on the flat as well as non-flat surfaces.

Liquid metal injection molding (LMIM) is a novel approach for patterning LM on the soft and stretchable substrate. It is analogous to plastic injection molding or metal injection molding (MIM) which involves melting the plastic or solid metal particles respectively. Subsequently, the feedstocks are then injected into the mold in liquid form using injection molding machines. After

it is detached from the mold, the material undergoes various operations such as drying and cooling for obtaining desired properties. The advantage of liquid metal is that it is liquid at room temperature, making it possible to inject it through a microfluidic metallophobic mold and connect it to the substrate. The metallophobic fumed silica coating prevents the adhesion of LM oxide with the mold which enables precise patterning of liquid metals geometries on the target substrate. The microfluidic mold here is not part of the final device. The present thesis introduces and authenticates a novel method of liquid metal injection molding (LMIM) for precise patterning of LM on various substrates with the use of the thermoplastic metallophobic microfluidic mold for their application in 3D printed electronics.

2.2 Materials and methods

2.2.1 Preparation of microchannel thermoplastic molds

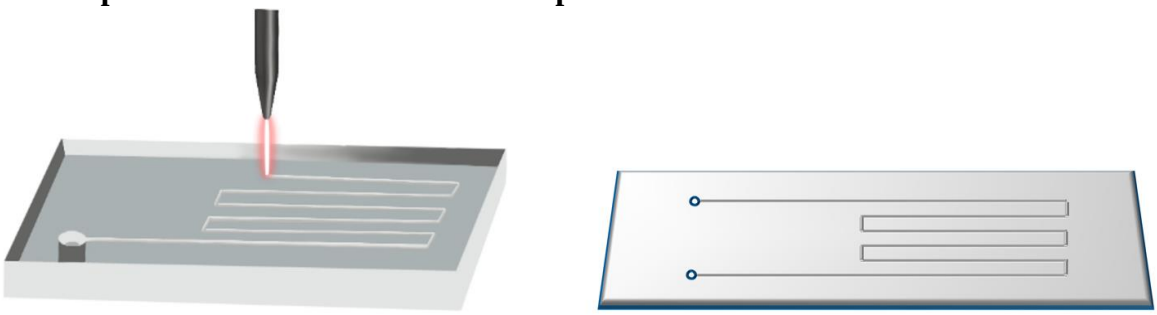

Figure 7: (a) Schematic of laser engraving of strain gauge shape microchannels on PMMA (b) Schematic of fabricated mold

The pre-designed microchannel geometries were ablated on thermoplastic acrylic sheets (PMMA) using a commercial laser writing system (VLS 3.50, Universal Laser System) with a 40 W CO_2 laser operating at 10.6 µm. The geometries engraved on the thermoplastics depend upon the operational parameter of the laser writer which comprises the speed and power. Here, we optimized the parameters as 30% power and 20% speed for patterning geometries of ~300 µm width. The present work demonstrates the use of thermoplastic for making the microchannel mold,

however, other materials can be used for the fabrication of the microchannel molds for the liquid metal printing process.

2.2.2 Metallophobic coating using fumed silica (FS)

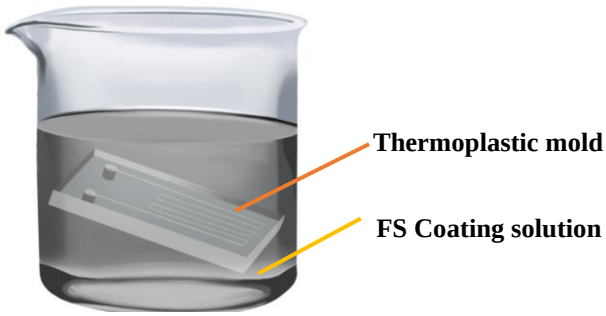

Figure 8: Schematic of fumed silica coating on the PMMA mold

Liquid metal oxide have the inherent quality of adhering to most surfaces, limiting their capacity to flow and shape stability. This can be eliminated by introducing roughness at the interface by developing metallophobic surfaces, researchers previously have used molding[16], etching[17], sputtering [18–20,] and spray coating[21,22] to make the surface metallophobic. Although these techniques are simple, they can only be used to coat exterior surfaces, which restricts their use for treating the walls of microfluidic channels. The LM oxide tend to adhere to the thermoplastic mold and therefore, the thermoplastic mold was coated with FS which has a larger surface area (~150 m^2/g) by using the sol-gel process [23]. The FS coating introduces a nanoscale roughness (3-10 nm) on the surface of molds by temporarily plasticizing and partially solubilizing the surface of the polymer with the solvent. The plasticization helps in making the surface tacky and polymer chains at the surface mobilize, this enables adhesion between the FS and the polymer surface. The initial experiments were performed by coating PMMA with the FS solution however other surfaces like glass or metal can be coated with FS by sol-gel process.

2.2.2.1 Solvent ratio optimization

The morphology of the fumed silica-coated thermoplastic mold was altered by varying the ratio of good solvent to poor solvent. The good solvent promotes making the mold or polymer surface tackier if used in correct proportion with the poor solvent but using a higher proportion of good solvent could also result in dissolving the polymer mold. However, using large quantity of poor solvent relative to the good solvent results in the optimal roughness to prevent the adhesion of LM oxide with the polymer surface but leads to insufficient robustness for multiple uses of the mold. Therefore, we characterized the morphology of the coated surface and optimized the concentration of the good and poor solvents. The coating solution was prepared by dissolving the nanoparticles in dichloromethane (DCM- good solvent) followed by the addition of isopropanol (IPA- poor solvent). The FS coating of the microchannel mold was found to be efficient in introducing the roughness over the interior walls of the channel resulting in the prevention of adhesion between the LM oxide and PMMA surface.

2.2.2.2 Characterization of FS coated mold

The FS coating of mold was done to introduce a nanometric surface roughness with a notion of preventing the oxide adhesion with the engraved walls.

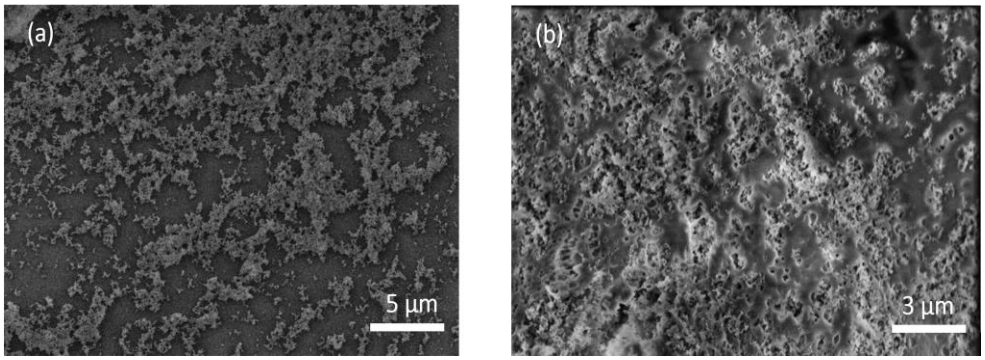

Figure 9: Scanning electron microscopy (SEM) images of (a) weakly bounded fumed silica (b) robustly bounded fumed silica on PMMA

Fumed silica can be actively dispersed in both good and poor solvents. An experiment was performed by using the poor solvent for dispersing FS and coating the polymer surface. Figure 9(a) demonstrates that if only poor solvent was used to coat FS on the polymer surface, the adhesion between the FS and the polymer surface was good enough to prevent the wetting of LM on the surface but was found to be lacking robustness on performing the test multiple times. Simultaneously, if only a good solvent is used for the coating, the FS is not at all coated on the surface instead the solvent dissolves the polymer and creates a porous structure. Therefore, the mixture of good and poor solvents in an appropriate ratio was used for the metallophobic coating of the polymer mold which yields both robustness and non-wettability. Figure 9(b) manifests the FS particle to be well adhered on the polymeric mold and yields non-wettability of LM on the surface. Previous work has reported that FS coating on the PMMA surface does not alter the transparency of the polymer[23]. However, the transparency of the PMMA changes upon the dissolution of the polymer surface. The dissolution of the polymer surface depends upon the ratio of the good solvent to the poor solvent.

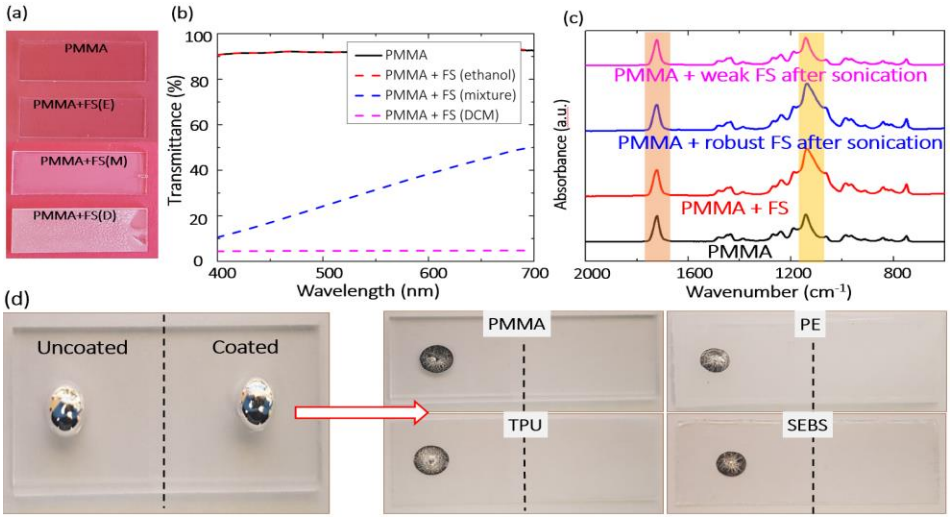

Figure 10: Optical images of PMMA with/without FS coating with varying ratios of good and poor solvents (b) UV -VIS spectra of the samples in the visible range (c) FT-IR spectra of the FS coated PMMA sample before and after sonication (d) Advancing and receding a liquid metal droplet on the coated substrate on the right side to test the adhesion of the LM oxide to various substrates with and without coating

Figure 10(a) and 10(b) demonstrates the change in the optical transparency with a different solvent and which is found to decreases with the increase in the proportion of the good solvent (DCM). The PMMA mold without coating and with FS (ethanol) coating has the highest transmissivity whereas the transmissivity drops with the addition of DCM. In the present work, we have tested different composition ratios of good solvent to poor solvent 1:1, 1:2, 1:3, 1:4, and 1:5. It was observed that composition with a 1:3 (% weight) ratio demonstrated optimum performance, and the PMMA mold was found to be almost transparent as with the increase in good solvent, the light scattering increases. Thereby, decreasing the transparency over the visible light range. The robust coating of FS on the polymer can be determined by conducting Fourier transform infrared spectroscopy in attenuated total reflection mode (FT-IR ATR) spectra. The FS-coated structure reflects stronger Si-O stretching intensity at 1100 cm^{-1} which is demonstrated by peaks in Figure 10(c) (black and red spectrum). The weakly bound FS coating can be easily removed by mechanical stimuli like bath sonication. As a result, the intensity of Si-O peak decreases clearly for the magenta plot (Figure 10(c)). On the other hand, if the FS coating is robust then the peak intensity will not change as shown by the blue graph. We have conducted experiments to demonstrate the robustness of the coating by partially coating the mold with FS solution followed by advancing and receding the LM droplet multiple times at the same spot as shown in Figure (d). While receding, the LM lefts behind the residue on the uncoated surface. However, even after multiple advancing and receding of LM drop, there was no residue found on the FS coated surface which suggests an advantage of patterning LM geometries multiple time with the same FS coated mold.

2.2.3 Injection of liquid metal

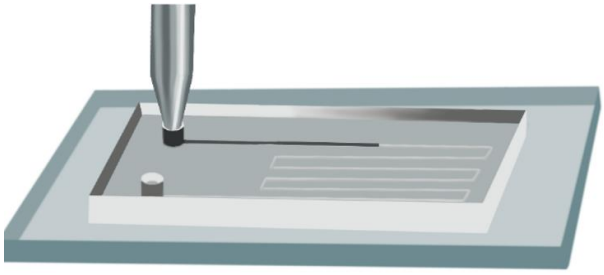

Figure 11: Schematic for injection of liquid metal into microfluidic channels.

The PMMA molds are fabricated with two holes that are used as an inlet and outlet for LM. The FS-coated mold has a roughness of nanometer scale, which is sufficient to prevent the adhesion of LM oxide with the polymer or mold surface. The FS coated mold is then placed on the substrate which needs to be patterned with LM geometries for its application in 3D electronics. The syringe or nozzle filled with the LM is used to inject the liquid metal through the microchannels. The LM is injected through the inlet holes with the pressure sufficient to break the oxide skin and it readily flows through microchannels and emerges out from the outlet hole.

2.2.4 Lifting off the mold

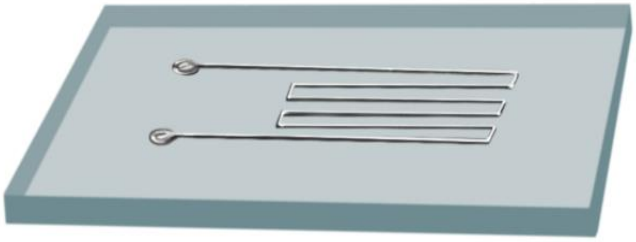

Figure 12*:* Schematic of a precise strain gauge patterned on lifting the mold off the substrate.

The final stage in the LMIM process for printing liquid metal geometries on different substrates is to lift off the metallophobic mold. Following the injection of liquid metal, the metallophobic mold must be carefully lifted off to obtain a precise pattern. Since the wall of

channels is FS coated, the roughness prevents the LM to get stuck with the walls. The LM will adhere strongly to the substrate providing a stable fine geometry or lines after lifting of the mold.

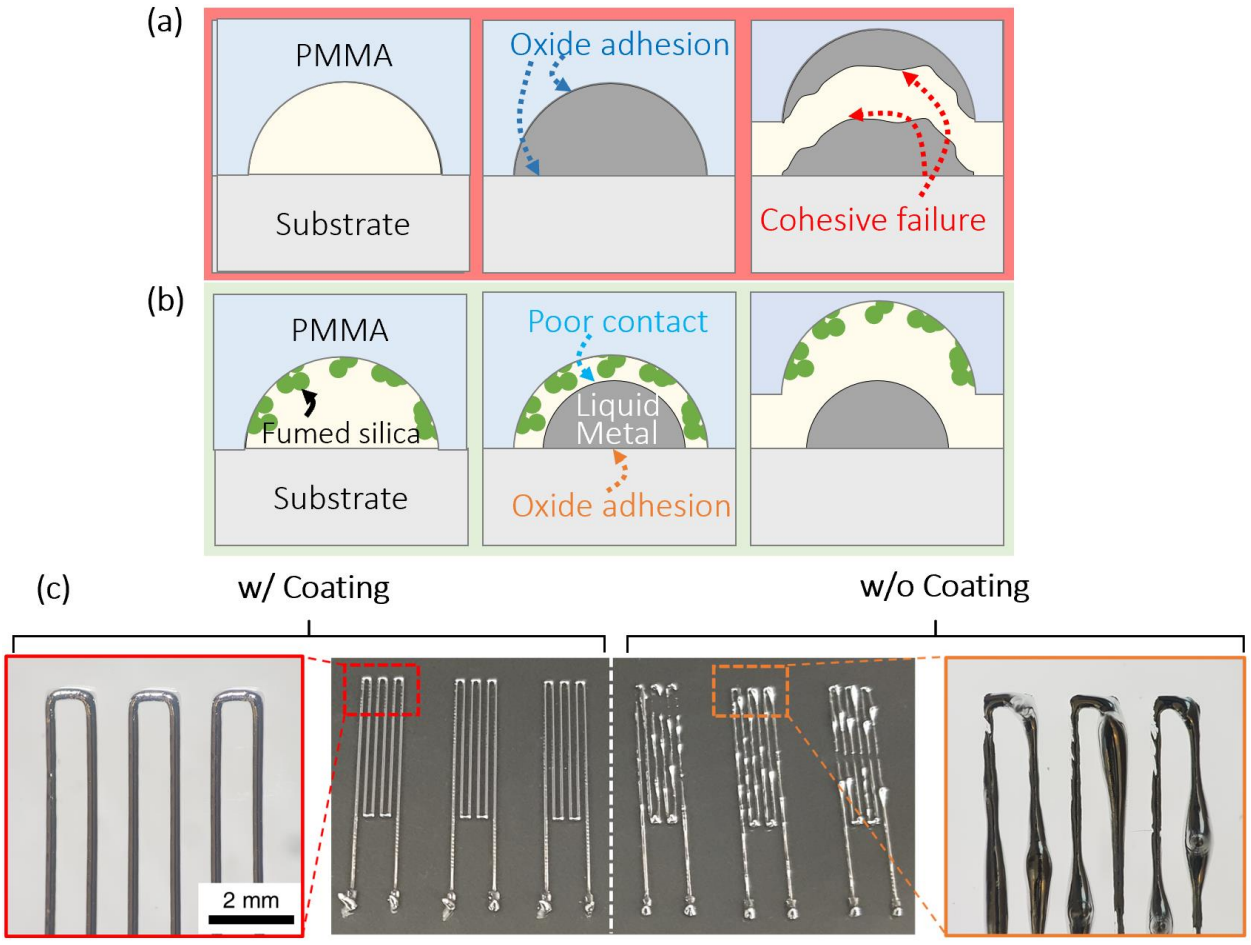

Figure 13: (a) Schematic demonstrating the cohesive failure of LM patterned geometry using the non-coated PMMA mold (b) Schematic showing roughness introduced by FS coating on mold prevents cohesive failure enabling smooth and precise patterning of LM on substrates (c) Snapshots of the strain gauge patterned on substrates using PMMA mold with and without FS coating

The Figure 13(a, b) demonstrates the lift-off step for the polymer mold with and without FS coating. The mold without the FS coating has a smooth surface, LM-filled microchannels cling to the wall. As a result, the LM oxide get adhered to the smooth surface of the mold during the lift-off stage leading to a cohesive failure which ultimately results in non-uniform patterns having a very high resistance value. However, the mold with FS coating has sufficient roughness to prevent

adhesion between the LM and the polymer surface which results in precise and reproducible patterns.

2.2 Surface independent patterning

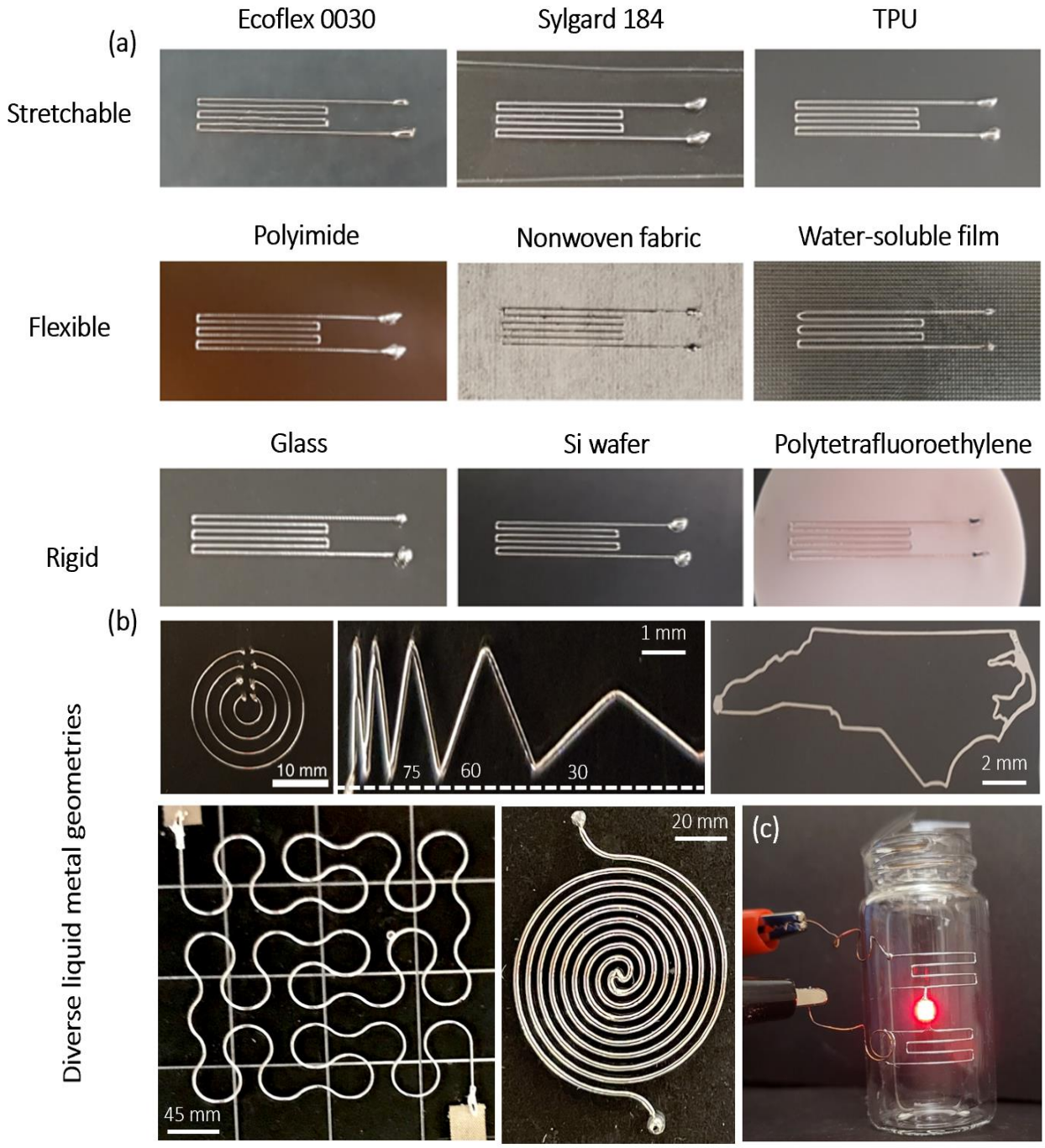

Figure 14: (a) A strain gauge LM was patterned on various substrates which make the method surface independent (b) various geometries were patterned independent of its geometrical parameters (c) Liquid metal circuit with LED was patterned on the curved surface

Liquid metal oxide readily adheres to most surfaces regardless of their chemical nature[24]. Hence, the LMIM method can use to print geometries on various substrates. The Figure 14(a) shows the strain gauge printed using the LMIM method on various types of stretchable, flexible, and rigid substrates. We conducted an experiment to verify the ability to inject print on different substrates and to do so repeatably. This included pattering strain gauge 50 times with a single polymer mold, with constant electrical resistance in all the patterns. The resistance value of all the strain gauge wires was around 1.38 Ω, which indicates wires were identical. The FS coating on the polymer is also durable enough for reproducible patterns with the same mold, demonstrating that LMIM is a highly consistent and reliable method. The minimum width of liquid metal lines achieved with this method was 100µm. Note that the linewidth also depends upon the geometries of microchannels on the thermoplastic molds. The resolution can be improved further by using a high-resolution laser for ablating microchannels on thermoplastics and a method of applying uniform pressure to the mold during liquid metal injection to prevent leaks from all sides of the mold.

As shown in the Figure LMIM is used for patterning various geometries with different widths, angles, and shapes. Unless and until the mold has two holes for inlet and outlet of liquid metals, liquid metal inject can be utilized to form diverse shapes like spiral coils, North Carolina boundary, serpentine, etc. The modulus of the substrate also affects the flow of LM via microchannels; hence the LM could be injected if the modulus of the substrate is lower than ~300 kPa patterning geometries. In the present study, as we used thermoplastic mold, it was also possible to pattern LM on curved surface as shown in Figure 14(c). PMMA mold was thermoformed with a glass vial at a temperature beyond the glass transition temperature. This mold was then placed on the curved surfaced glass vial and liquid metal was injected into the microchannels. After lifting

the mold carefully, a precise strain gauge pattern was obtained on the glass surface. A LED was attached to demonstrate its electrical connectivity of the strain gauge pattern. This makes liquid metal injection molding a potential method for printing 3D electronics.

2.3 Large scale printing of liquid metals

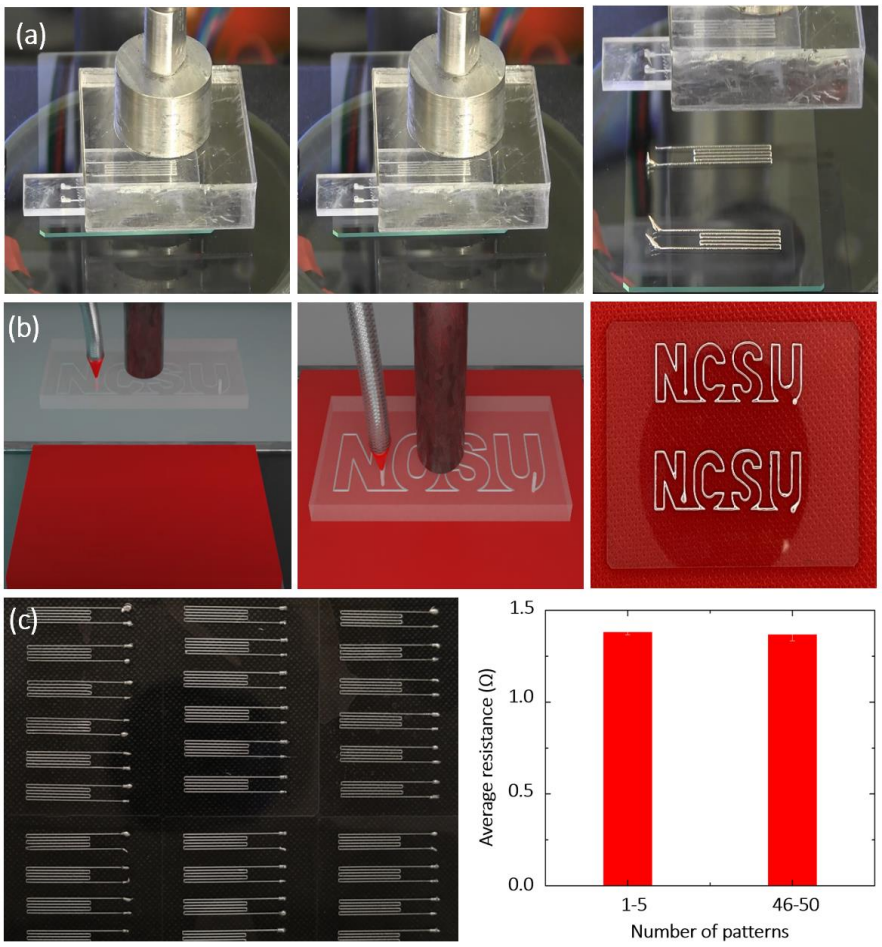

Figure 15: Large scale printing of (a) strain gauge (b) NCSU. The strain gauge was patterned 50 times and its resistance value was compared.

We conducted experiments to demonstrate that reusability of the mold for patterning. The mold was attached to a piston in a way that it does not cover the inlet and outlet holes of the mold for LM to flow. The mold was then placed on the substrates, followed by injection of liquid metal, and then lifting off of the mold. The process was repeated multiple times by arranging the substrate for multiple patterning of liquid metal. This demonstrates the durability of the non-stick coating

using the same mold repeatedly. As shown in the Figure 15(a, b), the strain gauge and NCSU patterns on the substrate were highly consistent and with identical cross-section. Figure 15 (c) compares the resistance values of 50 strain gauges to evaluate the uniformity of electrical properties.

2.4 Conclusion

We presented a new method for imprinting liquid metal that is repeatable, simple, and reliable. The current study addresses the disadvantages of using conventional injection to print liquid metal and demonstrates a new method of patterning LM. In contrast to earlier injection methods, the mold in LMIM does not become a part of the system, reducing the possibility of microchannel collapse and enabling the metals to be encased by a variety of polymers that differ in composition from the mold. Liquid metal injection molding can be used for mass scale printing of various geometries on flat as well as curved surfaces for its potential application in 3D microelectronic devices.

2.5 References

(1) CRC Handbook of Chemistry and Physics, 88th ed Editor-in-Chief: David R. Lide (National Institute of Standards and Technology) CRC Press/Taylor & Francis Group: Boca Raton, FL. 2007. 2640 pp. $139.95. ISBN 0-8493-0488-1. | Journal of the American Chemical Society. https://pubs.acs.org/doi/10.1021/ja077011d (accessed 2022-09-03).

(2) Microfluidic organ-on-chip system for multi-analyte monitoring of metabolites in 3D cell cultures - Lab on a Chip (RSC Publishing) DOI:10.1039/D1LC00689D. https://pubs.rsc.org/en/content/articlehtml/2022/lc/d1lc00689d (accessed 2022-09-03).

(3) Lu, T.; Markvicka, E. J.; Jin, Y.; Majidi, C. Soft-Matter Printed Circuit Board with UV Laser Micropatterning. ACS Appl. Mater. Interfaces **2017**, 9 (26), 22055–22062. https://doi.org/10.1021/acsami.7b05522.

(4) Abd, M.; Paul, R.; Aravelli, A.; Bai, O.; Lagos, L.; Lin, M.; Engeberg, E. Hierarchical Tactile Sensation Integration from Prosthetic Fingertips Enables Multi-Texture Surface Recognition. Sensors **2021**, 21, 29. https://doi.org/10.3390/s21134324.

(5) Fishel, J.; Loeb, G. Bayesian Exploration for Intelligent Identification of Textures. Front. Neurorobotics **2012**, 6.

(6) Othman, W.; Lai, Z.-H. A.; Abril, C.; Barajas-Gamboa, J. S.; Corcelles, R.; Kroh, M.; Qasaimeh, M. A. Tactile Sensing for Minimally Invasive Surgery: Conventional Methods and Potential Emerging Tactile Technologies. Front. Robot. AI **2022**, 8.

(7) Microfluidic electronics - Lab on a Chip (RSC Publishing) DOI:10.1039/C2LC21176A. https://pubs.rsc.org/en/content/articlehtml/2012/lc/c2lc21176a?casa_token=Hmz3s-g6svQAAAAA:tCz2CeYnv2jR-CltNxi_cy0DtBhGW6zZr4alEfO8eXTSIGBzXz_3hlm0n3Kkh3LicFAwbHuRrQFJVg (accessed 2022-09-03).

(8) The measurement of volume changes in human limbs - PMC. https://www.ncbi.nlm.nih.gov/pmc/articles/PMC1366051/ (accessed 2022-09-03).

(9) Fassler, A.; Majidi, C. Soft-Matter Capacitors and Inductors for Hyperelastic Strain Sensing and Stretchable Electronics. Smart Mater. Struct. **2013**, 22 (5), 055023. https://doi.org/10.1088/0964-1726/22/5/055023.

(10) Li, M.; Xiao, J.; Wu, J.; Kim, R.-H.; Kang, Z.; Huang, Y.; Rogers, J. A. Mechanics Analysis of Two-Dimensionally Prestrained Elastomeric Thin Film for Stretchable Electronics. Acta Mech. Solida Sin. **2010**, 23 (6), 592–599. https://doi.org/10.1016/S0894-9166(11)60006-2.

(11) Eutectic Gallium-Indium (EGaIn): A Liquid Metal Alloy for the Formation of Stable Structures in Microchannels at Room Temperature - Dickey - 2008 - Advanced Functional Materials - Wiley Online Library. https://onlinelibrary.wiley.com/doi/10.1002/adfm.200701216 (accessed 2022-08-08).

(12) High-Density Soft-Matter Electronics with Micron-Scale Line Width - Gozen - 2014 - Advanced Materials - Wiley Online Library. https://onlinelibrary.wiley.com/doi/abs/10.1002/adma.201400502 (accessed 2022-08-08).
(13) Khan, M. R.; Trlica, C.; Dickey, M. D. Recapillarity: Electrochemically Controlled Capillary Withdrawal of a Liquid Metal Alloy from Microchannels. Adv. Funct. Mater. **2015**, 25 (5), 671–678. https://doi.org/10.1002/adfm.201403042.
(14) Lu, T.; Finkenauer, L.; Wissman, J.; Majidi, C. Rapid Prototyping for Soft-Matter Electronics. Adv. Funct. Mater. **2014**, 24 (22), 3351–3356. https://doi.org/10.1002/adfm.201303732.
(15) Gallium-based liquid metal inkjet printing. https://ieeexplore.ieee.org/document/6765804/ (accessed 2022-09-03).
(16) A Super-Lyophobic 3-D PDMS Channel as a Novel Microfluidic Platform to Manipulate Oxidized Galinstan | Semantic Scholar. https://www.semanticscholar.org/paper/A-Super-Lyophobic-3-D-PDMS-Channel-as-a-Novel-to-Kim-Lee/1d3b36ea9191b990bef1b66a51e46052836e9703 (accessed 2022-09-03).
(17) Kadlaskar, S. S.; Yoo, J. H.; Abhijeet, null; Lee, J. B.; Choi, W. Cost-Effective Surface Modification for Galinstan® Lyophobicity. J. Colloid Interface Sci. **2017**, 492, 33–40. https://doi.org/10.1016/j.jcis.2016.12.061.
(18) Kramer, R. K.; Majidi, C.; Wood, R. J. Masked Deposition of Gallium-Indium Alloys for Liquid-Embedded Elastomer Conductors. Adv. Funct. Mater. **2013**, 23 (42), 5292–5296. https://doi.org/10.1002/adfm.201203589.
(19) Kramer, R. K.; Boley, J. W.; Stone, H. A.; Weaver, J. C.; Wood, R. J. Effect of Microtextured Surface Topography on the Wetting Behavior of Eutectic Gallium-Indium Alloys. Langmuir ACS J. Surf. Colloids **2014**, 30 (2), 533–539. https://doi.org/10.1021/la404356r.
(20) Agarwal, A.; Tomozawa, M. Correlation of Silica Glass Properties with the Infrared Spectra. J. Non Cryst. Solids **1997**, 209, 166–174. https://doi.org/10.1016/S0022-3093(96)00542-X.
(21) Joshipura, I. D.; Ayers, H. R.; Castillo, G. A.; Ladd, C.; Tabor, C. E.; Adams, J. J.; Dickey, M. D. Patterning and Reversible Actuation of Liquid Gallium Alloys by Preventing Adhesion on Rough Surfaces. ACS Appl. Mater. Interfaces **2018**, 10 (51), 44686–44695. https://doi.org/10.1021/acsami.8b13099.
(22) Yao, Y. Y.; Ding, Y. J.; Li, H. P.; Chen, S.; Guo, R.; Liu, J. Multi-Substrate Liquid Metal Circuits Printing via Superhydrophobic Coating and Adhesive Patterning. Adv. Eng. Mater. **2019**, 21 (7), 1801363. https://doi.org/10.1002/adem.201801363.
(23) Ma, J.; Bharambe, V. T.; Persson, K. A.; Bachmann, A. L.; Joshipura, I. D.; Kim, J.; Oh, K. H.; Patrick, J. F.; Adams, J. J.; Dickey, M. D. Metallophobic Coatings to Enable Shape Reconfigurable Liquid Metal Inside 3D Printed Plastics. ACS Appl. Mater. Interfaces **2020**. https://doi.org/10.1021/acsami.0c17283.

(24) Daeneke, T.; Khoshmanesh, K.; Mahmood, N.; Castro, I. A. de; Esrafilzadeh, D.; Barrow, S. J.; Dickey, M. D.; Kalantar-zadeh, K. Liquid Metals: Fundamentals and Applications in Chemistry. Chem. Soc. Rev. **2018**, 47 (11), 4073–4111. https://doi.org/10.1039/C7CS00043J.

CHAPTER 3

APPLICATIONS

3.1 Introduction

Liquid metal injection molding (LMIM) is a promising method for printing various geometries for applications in soft and stretchable electronic devices. The electrical, mechanical, and thermal properties of the liquid metal geometries make it important for its potential use in soft circuits, wearable heaters, soft actuators, and soft robotic applications. The present chapter provides a brief overview of the use of the LMIM method for patterning LM geometries for applications in soft and wearable electronic devices.

3.2 Stretchable wires

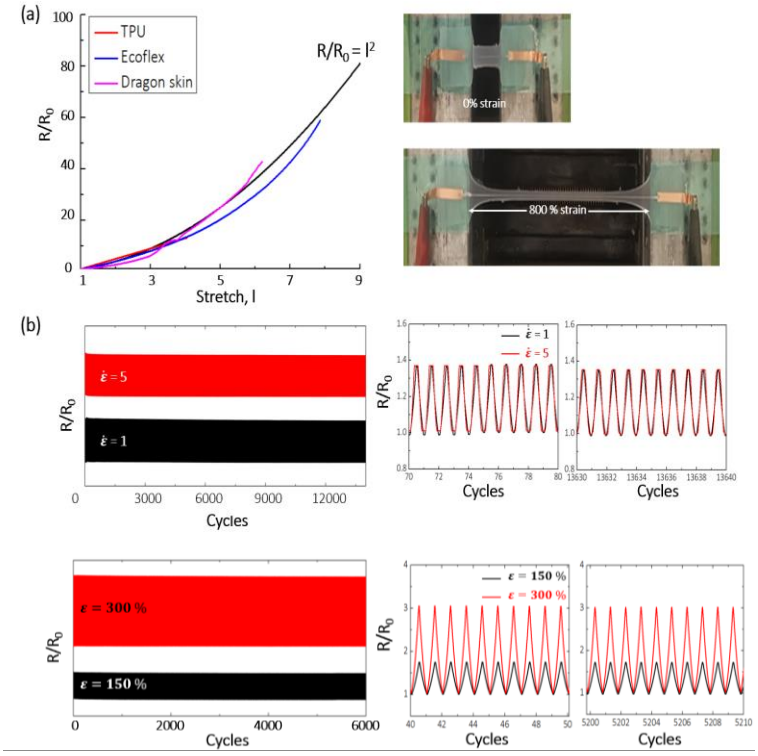

Figure 16: The electro-mechanical properties of stretchable liquid metal wires created by injection molding. (a) Strain-resistance curve for different elastomer substrates (b) Cyclic test of stretchable LM wires.

LM wires can be employed as interconnects between circuits elements [1–6]. Patterned LM shows highly stable electro-mechanical properties as long as the substrates embedding the LM is elastic. As shown in Figure 16(a), the resistance value of the wire increases as the LM wire encapsulated in the elastomers was stretched. The resistance value of the strechable wire was directly proportional to the square of the strain, $\boldsymbol{\lambda = \varepsilon + 1}$ where ε is elongated length/actual length, following the Pouilet's equation since the volume of the liquid metal is conserved while stretching. The resistance of LM wire increases by 64 times at 800% strain to (~30 Ω from its initial value) of 0.55 Ω Ω at zero strain. This increase occurs due to elongation of the length and narrowing of the cross-section of the wire during elongation. The LM wires encapsulated in the elastomer were tested mechanically and electrically, these wires tends to fail only when the substrates failed mechanically. Along with the stretchability of LM wires, the cycalibility is also crucial to ensure the robustness and consistency of the stretchable electrodes or wires. As shown in Figure, experiments were conducted by patterning the LM wire and encapsualting it in a commercially available elastomer (Ecoflex 0030) as an initial substrate material. Ecoflex0030 has high stretchability, elasticity and negligible mechanical hystresis up to ~300% of the strain. Initially, we stretched and released the liquid metal wire encapsultaed in elatomer to 100% strain with two different strain conditions (100%/s or 500%/s). The resistance value for both the case were identical over 12k cycles and there were no changes found in cyclability of LM wire and the substrate. Formation of oxide was evident from the wrinkles formed on the surface of the LM and from the loss of the shiny surface of LM. As expected, the resistance value of the LM wire did not change after 6000 strain cycles. The experiments were terminated in either of the case when the elastomer eventually failed due to mechanical fatigue, however the electrical conductivity did not change until the elastomer failed completely.

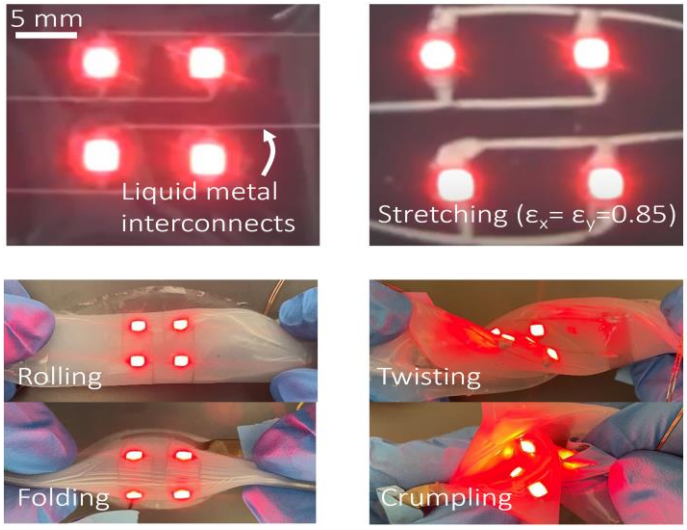

Figure 17: Application of stretchable wires, highly deformable 2×2 LED array is embedded in elastomers.

An array of LEDs was used as a demonstration of the durability of the LM patterned wires.. This serve as an important practical application to visually confirm the structural integrity of a circuit under mechanical deformation. Because of this stabilty, the circuit consisting array of LEDs remains functional when rolled, folded, twisted and crumpled. This also demonstrates the stretchability and durability of LM wires patterned by LMIM.

3.3 Wearable heaters

Wearable electrically driven heaters based on Joule heating are useful [7–13]. Due to its compliant nature, the heating of soft matter has been adopted for its application in material intelligence, sensors, thermotherapy[14–17], and other medical applications. In this work, we fabricate and characterize the performance of the soft wearable heater fabricated using liquid metal injection molding. The fabrication process involves patterning of LM wire on PDMS substrate, followed by its encapsulation with additional cured polymer. The LM wire ends are connected with the external electrodes to a DC voltage supply. The notion was to test the stability of the LM

base soft heater by tuning the current input to obtain the desired temperature range for its application in thermotherapy.

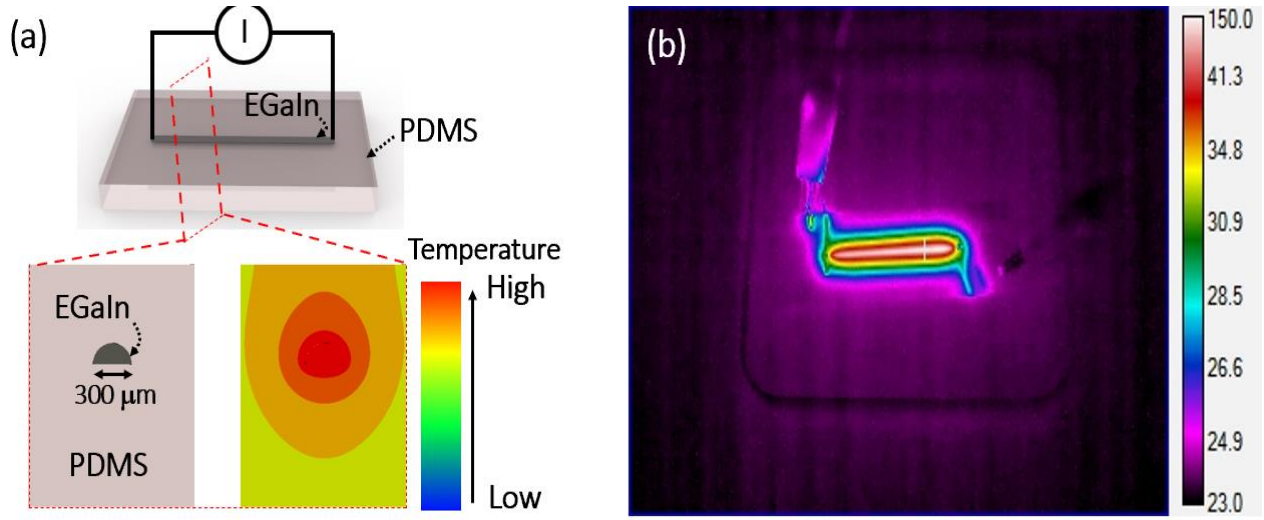

Figure 18: (a) Schematic of the Joule heating experiment where a LM wire was patterned and encapsulated into an elastomer. The temperature distribution was measured at different value of the current (b) Thermal imaging of the LM wire encapsulated in elastomer when 1.0 A current was applied.

As shown in the Figure 18(a), the initial experiments were performed by patterning LM wire with of width about 300 µm, length of 40 mm, and semi-circle crossectional geometry. The temperature of the PDMS surface was detected by using a thermal imaging camera (FLIR). The Joule heat generated is directly proportional to the square of the input value of current and therefore the temperature rises reasonably at a steady state. The temperature on the surface increases for a few minutes until it reaches to its steady state. The average time required for reaching a steady state was measured to be about 3 minutes. However, this duration also depends on the thickness, thermal conductivity, density, and heat capacity of the elastomer matrix. The experiments were successfully performed for current density up to ~ 5 kA/cm^2 i.e. 1.75 A current input without any sort of failure. The amplitude of current density here is pretty higher than the previously reported work. The thermal imaging camera utilized for temperature measurement had a temperature monitoring limit of up to 150 ^{o}C and therefore, the surface temperature higher than 150 ^{o}C was not

measured. However, the steady-state temperature determined by simulation at a current density of 5 kA/cm^2 was 205 ^{o}C. The liquid metal wire encapsulated into PDMS was found to loose its electrical conductivity above 5 kA/cm^2.

(a)

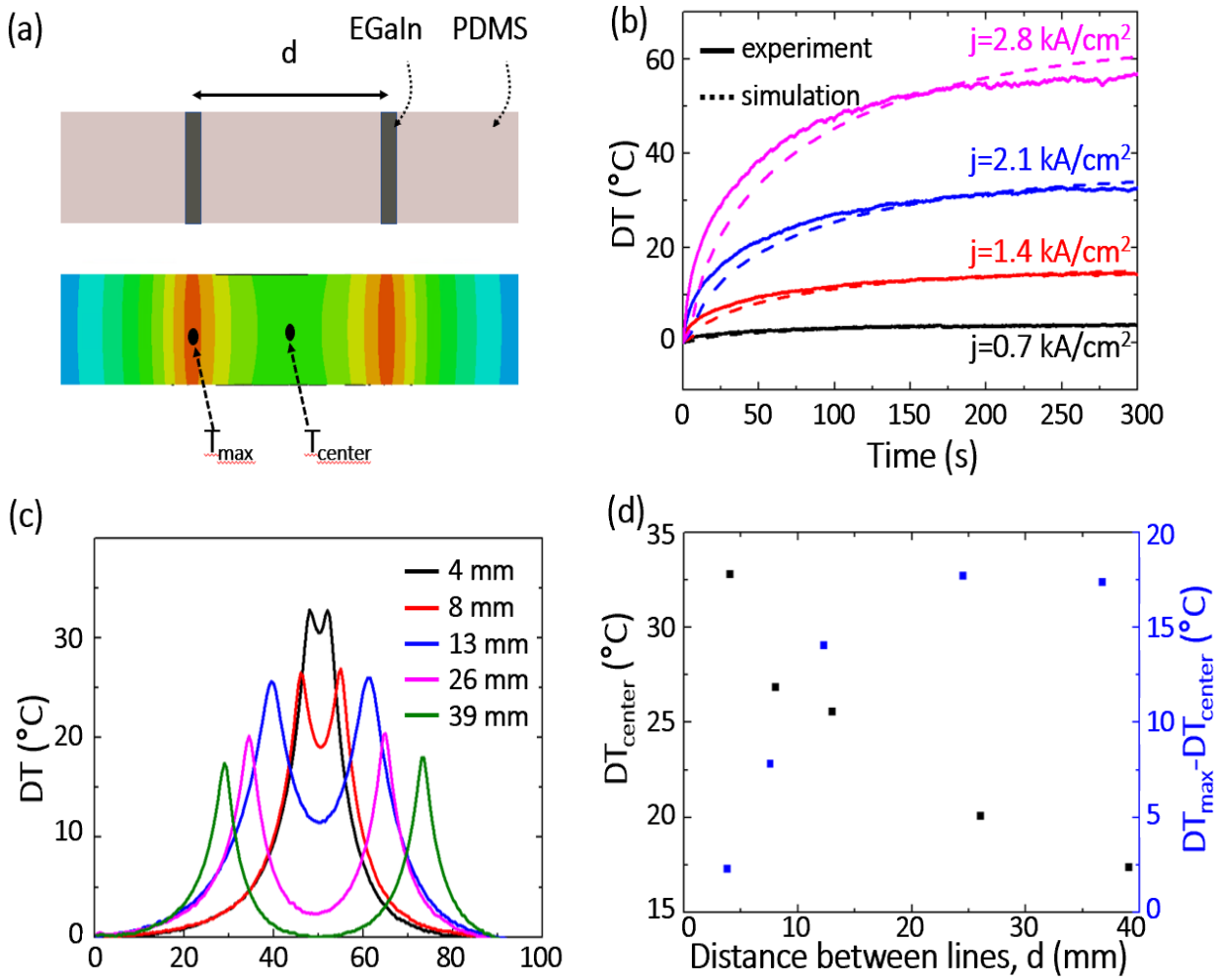

Figure 19: (a) Schematic of the Joule heating effect with two parallel lines encapsulated in an elastomer (b) Transient plot for measuring the temperature distribution with respect to time. The dashed lines are a representation of data from the FEM simulation and the solid lines represent the experimental data. (c) Spatial plot for the temperature difference between the lines printed at various distances. (d) Plot representation of the temperature difference at the center and the difference between the maximum point and the center point.

The simulation was carried out using the finite element method (FEM) to measure the temperature over time for different current density values. The simulation and experimental results for transient and stable states are closely related as shown in Figure 19(b). The experimental data closely matches the simulation results, highlighting the consistency and dependability of the

LMIM patterned geometries. The experimental data was limited to 150 ^{o}C while the simulation data was used to predict the temperature value for applied current density. The distribution of heat also depends upon the distance between the patterned lines. The distance between lines needs to be optimized to eliminate temperature hotspots and have a uniform temperature field over the area. To optimize the distance between patterned lines, multiple LM wires were patterned by the LMIM method to generate uniform temperature distribution across the area. The temperature distribution between two 40 mm long, 300 µm wide patterned wires was carried out at varying distances. Figure 19(c) demonstrates that as the distance between two patterned wires decreases, the temperature at the center point between the two lines increases due to interference of the temperature fields of patterned wires with each other. The temperature difference between the center point and each patterned line was 2.3, 7.86, 14.1, 17, 17 ^{o}C (top to bottom) and the distance between patterned lines was 4, 8, 13, 16, and 39 mm respectively. As shown in the Figure the interference of temperature fields starts to happen when the distance between two lines gets smaller than 13 mm. The data manifests that the shorter the distance between the patterned lines more is the interference of the temperature field, and the more uniform the temperature distribution. If the tolerance range for the temperature difference is set to 2.3 ^{o}C then 4 mm can be adopted as the optimized distance between two lines to avoid any significant temperature gradient and provide uniform heat distribution. The optimized distance between the two parallel patterned lines can be potentially used in patterning different geometries to enhance the performance of the wearable heaters

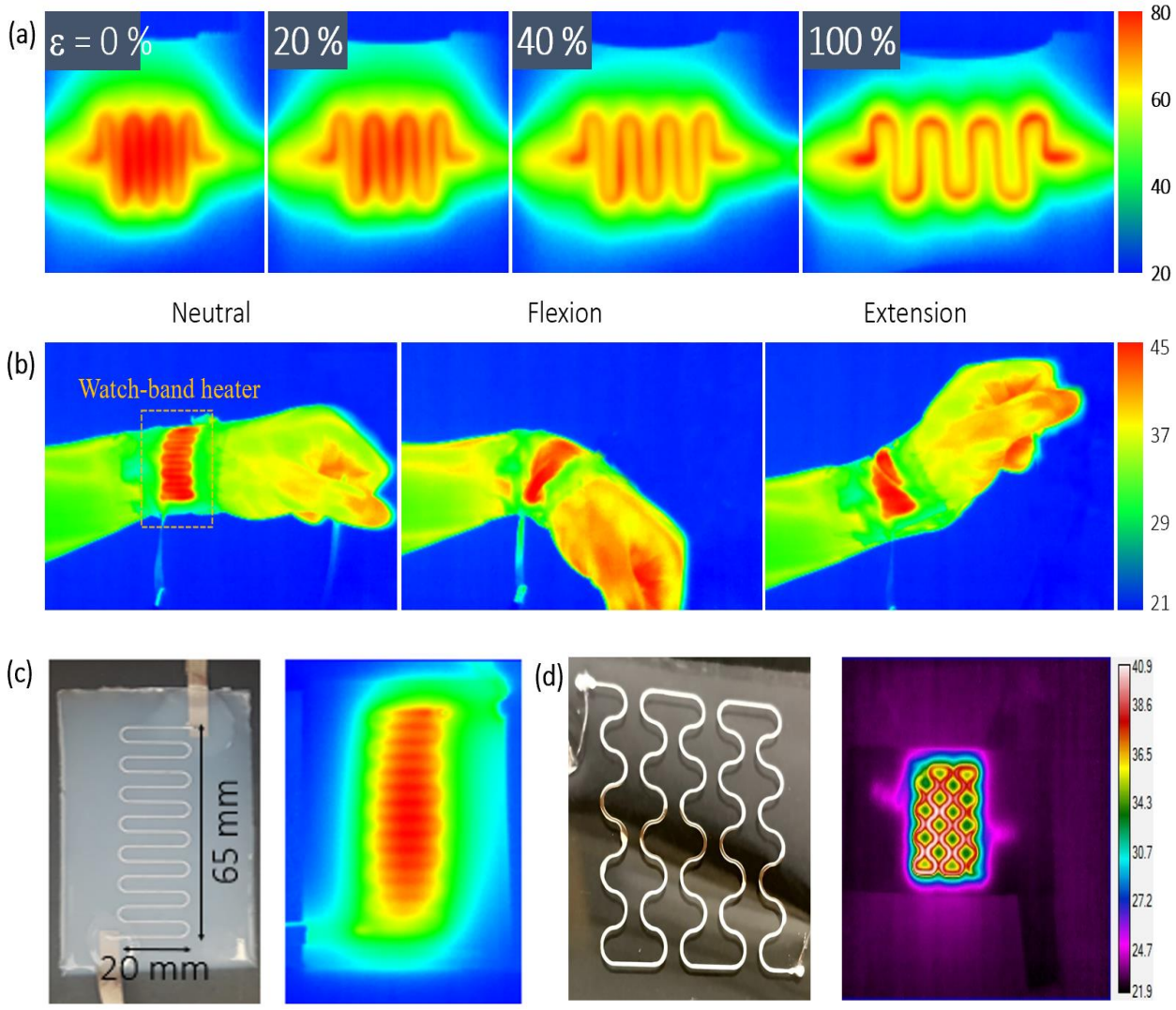

Figure 20: (a) Thermal imaging of the soft heater while stretching (b) Testing the soft heater with various modes of deformation (c) Optical image of soft heater and thermal image on application of 0.5 A current (d) optical and thermal imaging of the serpentine patterned soft heater.

Employing a 4 mm gap between the parallel lines, we have fabricated a wearable soft heater using the LMIM method to pattern different geometries that can be potentially used in for thermal therapy and health monitoring sensors. The liquid metal was injected through a microchannel mold to print a serpentine pattern as shown in Figure 20(c) to minimize the resistance change while stretching. The LM patterns were made on the TPU polymer film which was then encapsulated with additional elastomer. The conductive nylon fibers were used as external electrodes for the DC power supply. The fabricated soft heater was highly stretchable and did not show any

disconnection owing to the compliance of the liquid metal under strain. The soft heater band was worn on the wrist as depicted in Figure 20(b) and its temperature was adjusted to be slightly higher than the body temperature (40-45 ^{o}C) which is generally the case for thermal therapy, The temperature across the heater band was controlled by finely tuning the current input value. The heater's properties were then tested and it was observed that it does not show any discontinuous functioning during wrist deformation modes, including extension and flexion. The current input value for the wrist band heater was 0.5 A yielding a temperature range around 40-45 ^{o}C. The LMIM method was used to pattern other convoluted geometries to optimize the performance of the soft heater for its application in thermotherapy and other health monitoring devices.

3.4 Electroadhesion based soft device and grippers

In recent years, there has been an increase in the number of research works involving electroadhesion forces for soft actuators applications[18–20]. Electroadhesion employs an adhesion mechanism that involves the generation of adhesion force by applying high voltage. The electroadhesion system generates forces that help in handling irregular, rough surfaces, soft and fragile objects. In comparison to other adhesive forces, electroadhesion devices offer lightweight and high compliance properties due to the flexible film structure[21–24]. The electroadhesion devices also generate non-contact force that enhances the adaptability towards uneven and porous materials [25]. Electroadhesion can be triggered by simply turning on the high-voltage supply which reduces various complexities associated with the operation[26]. The electroadhesion with all its advantage has been employed in various sectors such as wafer transportation and processing of semiconductors[27], adhesion mechanism for climbing robots, electroadhesive grippers [28,29], and effectors for conducting space missions[30–34], The present work involves incorporating the liquid

metal electrodes to be used as electroadhesion device and soft grippers for its application in soft robotics. The electroadhesion forces were utilized to hold soft as well as fragile objects effectively which can be an interesting application in soft robotics.

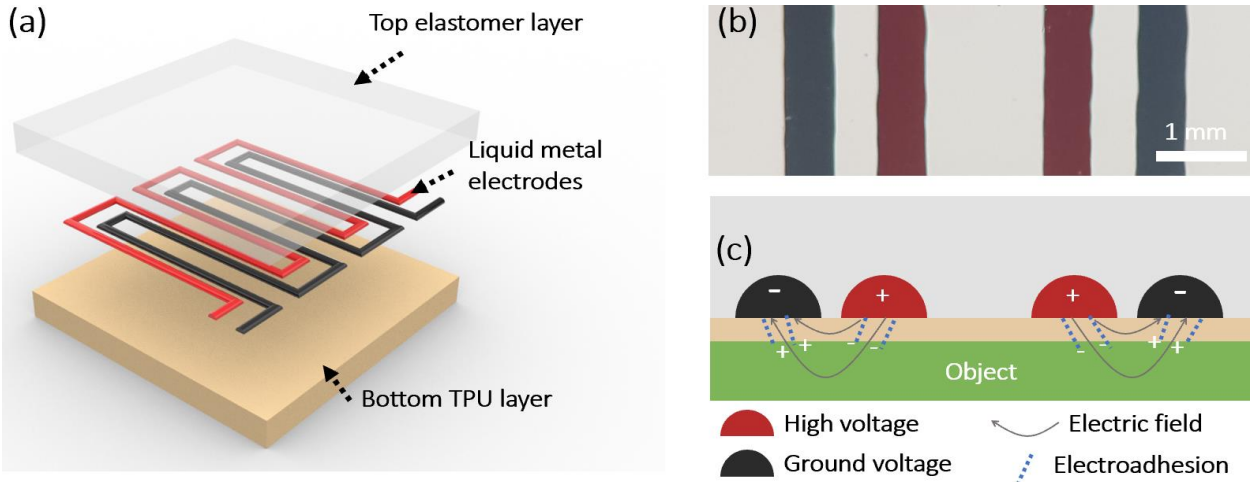

Figure 21: (a) Schematics of the electro adhesion and gripper device using LM electrodes (b, c) optical image of the two electrodes for electroadhesion

The experiments to demonstrate the electroadhesion phenomenon using liquid metal electrodes involves the fabrication of a device that utilizes high voltage values across the electrode to generate a strong adhesion force between electrodes and the object surface. The device includes the patterning of two electrodes on a 40µm thick TPU film followed by encapsulation with the Ecoflex 0030 as shown in Figure 21(a). The red electrode was applied with a high voltage value (up to 4 kV, 40 V/µm) and the black electrodes were grounded. The liquid metal electrodes were printed using the LMIM method and the distance between the red electrode lines and black electrode lines were kept at about 400 µm. Figure 21(b) shows a schematic representation of the black and red electrodes which generate a strong electric field on the application of a high value of voltage. The device was designed to lift soft as well as fragile objects by controlling the voltage input. When a high voltage is applied to the device, a strong electric field is created, which causes an object to become polarized. The polarized object and the electrodes are then subjected to a

powerful electrostatic force. As the polarized object and the electrodes are brought closer, the generated electrostatic force gets sufficiently strong to hold them together shown in Figure 21(c). This adhesion between the polarized object and the electrodes was harnessed to lift and drop the objects at varying heights. The object used here provides versatility in terms of thickness, weight, softness, and brittleness. The notion was to demonstrate to harness electrically driven adhesion for its compatibility with different objects.

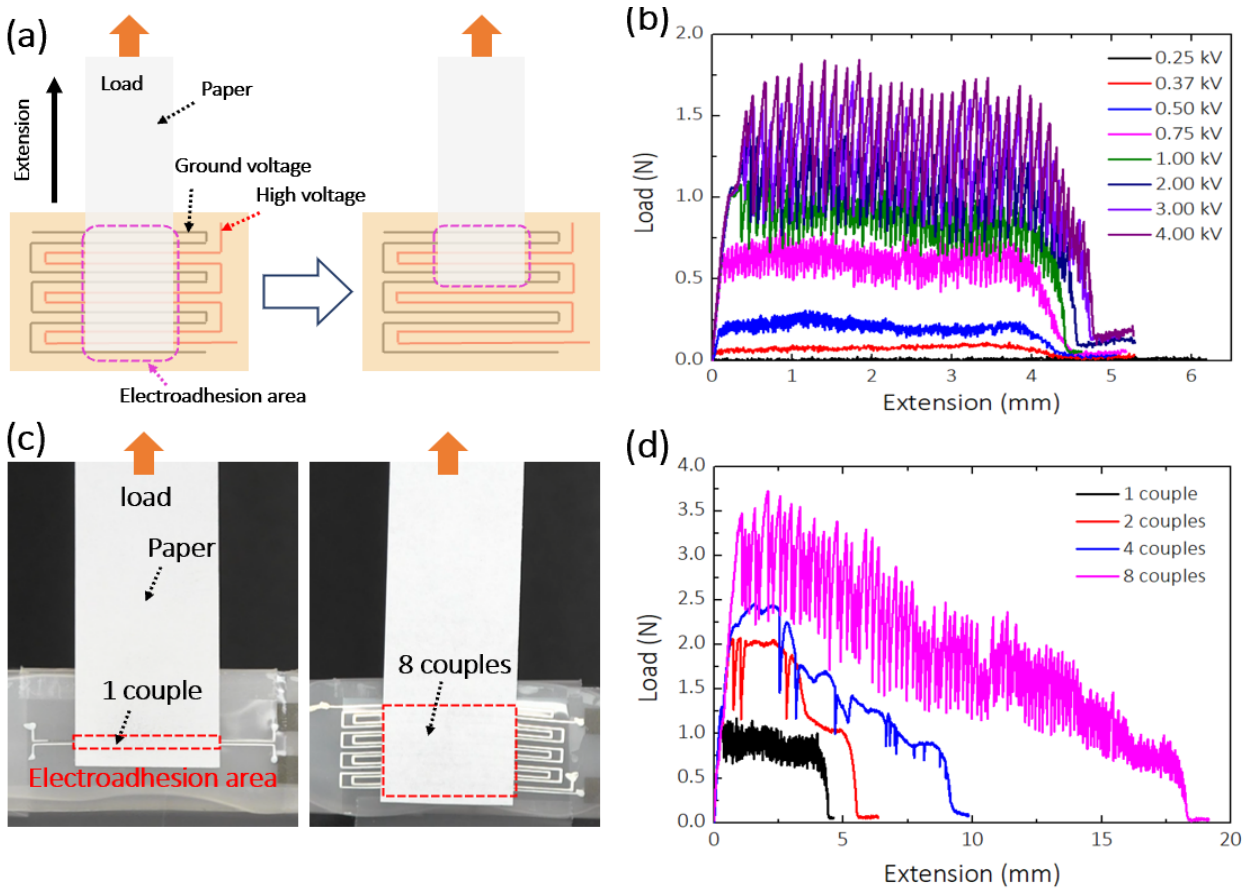

Figure 22: (a) Schematic for using measuring the shear forces using the paper as specimen (b) Extension-load curve for 1 couple with varying voltage values (c) Snapshot of the measurement of the shear force using different couples of LM electrodes (d) Extension-load curve for 1 kV with varying electrode couples.

To study the shear forces acting between the polarized object and the electrodes, a 25 mm wide paper strip was used as a specimen. We pulled it from the bottom to the top direction of the device while measuring the force using the tensile tester (Instron) as shown in Figure 22(a). The

shear force is comprised of the electro-shear force and the friction force between the device and the polarized object. The measurement was found to be complex as it was difficult to deconvolute the two forces and the friction force is highly dependent on the interfacial materials. If glass was used instead of paper, due to high friction it would be difficult to measure the forces accurately and hence paper is widely used to eliminate the intrinsic adhesion between the surface of the object and the electrode substrates. The friction between the paper and TPU film was found to be an almost negligible Figure 22(b) manifests that the shear force increases with increasing the values of voltage. The maximum force measured was 1.7 N at 4kV, considering the adhesion area (25mm x 1mm) shear force was found to be compared according to the previously reported work. If the number of electro-adhesion couples increases, the adhesion area interacting with the object increases, and hence the shear force increases. Figure 22(d) demonstrates the relation between the forces measured with extension for different number couples. The electro adhesion area decreases with pulling the paper out as the paper is pulled towards the top direction, and the contact between the couples and the paper starts reducing due to which the electroadhesion area decreases and so do the shear forces. The experiments provide credential over increase in the shear force with an increase in the electro adhesion area, the voltage applied, and an increase in the number of the couples. The findings demonstrate that having more electroadhesion couples increases the shear forces acting at the interface between object and film. The weight of the device was about 50 g and theoretically, the device can hold an object weighing 8 times heavier than the device itself.

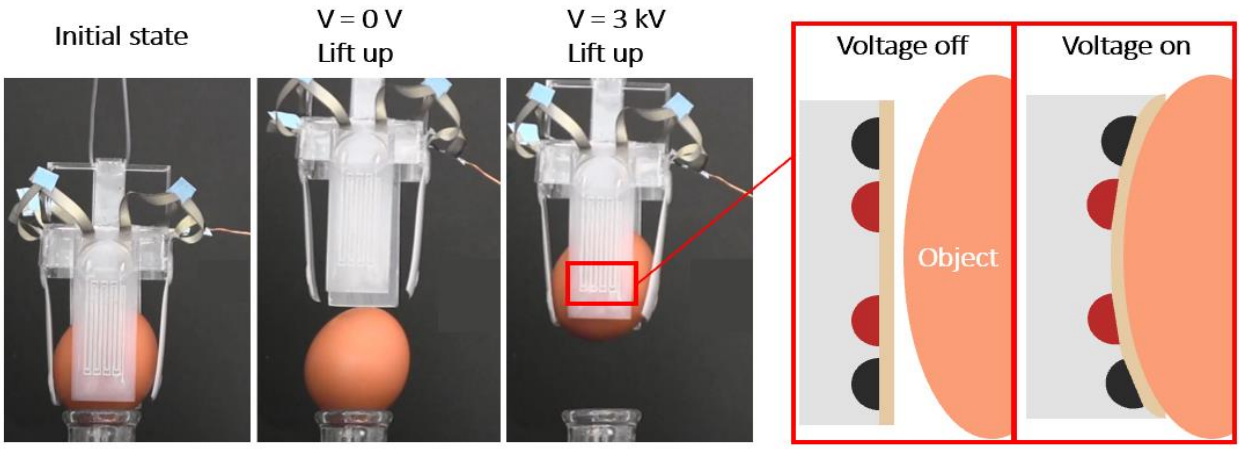

Figure 23: Soft grippers used for lifting object on application of the voltage

To harness the electroadhesion forces, we fabricated a soft and flexible gripper to grab and move an object. As shown in the Figure, an egg weighing about ~60g was used as a specimen to demonstrate the application of the electro-adhesion force for handling a curved object. The experiment involves four electro adhesion devices attached to exoskeletal PMMA pieces and the electrodes were externally connected with the high voltage supply. Figure 23(a) shows that the gripper does not grab the object without the application of voltage as such there are no electrostatic forces responsible for the adhesion of the object and the device. However, when 3 kV of voltage was applied to the liquid metal electrodes, the gripper gets adhered to the object's surface and grabbed the object. The adhesion force was sufficiently strong to hold and move the object around without dropping it. One of the key benefits of this gripper is the weak normal force and in terms of magnitude, the normal forces are two orders weaker than the shear force. When high voltage is applied, the grippers wrap around the object and due to weak normal forces, the grippers gently grab the object which eliminates the threat to break fragile objects. The grippers can be controlled with the application of voltage and hence can be used to move around the objects in a controllable way. The grippers utilizing the electro adhesion forces can be good potential solutions for handling soft, uneven, and fragile objects.

3.5 References

(1) Dorsey, K. L.; Lazarus, N. Lifetime of Liquid Metal Wires for Stretchable Devices. *Adv. Mater. Technol.* **2021**, *6* (4), 2001100. https://doi.org/10.1002/admt.202001100.

(2) Li, G.; Wu, X.; Lee, D.-W. Selectively Plated Stretchable Liquid Metal Wires for Transparent Electronics. *Sens. Actuators B Chem.* **2015**, *221*, 1114–1119. https://doi.org/10.1016/j.snb.2015.07.062.

(3) Zhu, S.; So, J.-H.; Mays, R.; Desai, S.; Barnes, W. R.; Pourdeyhimi, B.; Dickey, M. D. Ultrastretchable Fibers with Metallic Conductivity Using a Liquid Metal Alloy Core. *Adv. Funct. Mater.* **2013**, *23* (18), 2308–2314. https://doi.org/10.1002/adfm.201202405.

(4) Li, M.; Wu, Y.; Zhang, L.; Wo, H.; Huang, S.; Li, W.; Zeng, X.; Ye, Q.; xu, tianbai; Dong, S.; Li, Y.; Jin, H.; Wang, X. Liquid Metal Based Electrical Interconnects and Interfaces with Excellent Stability and Reliability for Flexible Electronics. *Nanoscale* **2019**, *11*. https://doi.org/10.1039/C8NR09503E.

(5) Park, C. W.; Moon, Y. G.; Seong, H.; Jung, S. W.; Oh, J.-Y.; Na, B. S.; Park, N.-M.; Lee, S. S.; Im, S. G.; Koo, J. B. Photolithography-Based Patterning of Liquid Metal Interconnects for Monolithically Integrated Stretchable Circuits. *ACS Appl. Mater. Interfaces* **2016**, *8* (24), 15459–15465. https://doi.org/10.1021/acsami.6b01896.

(6) Li, M.; Wu, Y.; Zhang, L.; Wo, H.; Huang, S.; Li, W.; Zeng, X.; Ye, Q.; Xu, T.; Luo, J.; Dong, S.; Li, Y.; Jin, H.; Wang, X. Liquid Metal-Based Electrical Interconnects and Interfaces with Excellent Stability and Reliability for Flexible Electronics. *Nanoscale* **2019**, *11* (12), 5441–5449. https://doi.org/10.1039/C8NR09503E.

(7) Ha, S.-H.; Kim, J.-M. Rapid and Economic Preparation of Wearable Thermotherapy Pad Based on Simple Cut-Patterning of Metal Foil Supported by Plastic Sheets. *RSC Adv.* *11* (2), 918–926. https://doi.org/10.1039/d0ra05728b.

(8) Liu, Q.; Huang, J.; Zhang, J.; Hong, Y.; Wan, Y.; Wang, Q.; Gong, M.; Wu, Z.; Guo, C. F. Thermal, Waterproof, Breathable, and Antibacterial Cloth with a Nanoporous Structure. *ACS Appl. Mater. Interfaces* **2018**, *10* (2), 2026–2032. https://doi.org/10.1021/acsami.7b16422.

(9) Choi, S.; Park, J.; Hyun, W.; Kim, J.; Kim, J.; Lee, Y. B.; Song, C.; Hwang, H. J.; Kim, J. H.; Hyeon, T.; Kim, D.-H. Stretchable Heater Using Ligand-Exchanged Silver Nanowire Nanocomposite for Wearable Articular Thermotherapy. *ACS Nano* **2015**, *9* (6), 6626–6633. https://doi.org/10.1021/acsnano.5b02790.

(10) Cheng, Y.; Zhang, H.; Wang, R.; Wang, X.; Zhai, H.; Wang, T.; Jin, Q.; Sun, J. Highly Stretchable and Conductive Copper Nanowire Based Fibers with Hierarchical Structure for Wearable Heaters. *ACS Appl. Mater. Interfaces* **2016**, *8* (48), 32925–32933. https://doi.org/10.1021/acsami.6b09293.

(11) Fan, J. A.; Yeo, W.-H.; Su, Y.; Hattori, Y.; Lee, W.; Jung, S.-Y.; Zhang, Y.; Liu, Z.; Cheng, H.; Falgout, L.; Bajema, M.; Coleman, T.; Gregoire, D.; Larsen, R. J.; Huang, Y.; Rogers, J. A. Fractal Design Concepts for Stretchable Electronics. *Nat. Commun.* **2014**, *5*, 3266. https://doi.org/10.1038/ncomms4266.

(12) Niu, B.; Yang, S.; Hua, T.; Tian, X.; Koo, M. Facile Fabrication of Highly Conductive, Waterproof, and Washable e-Textiles for Wearable Applications. *Nano Res.* **2021**, *14* (4), 1043–1052. https://doi.org/10.1007/s12274-020-3148-3.

(13) Zhang, M.; Wang, C.; Liang, X.; Yin, Z.; Xia, K.; Wang, H.; Jian, M.; Zhang, Y. Weft-Knitted Fabric for a Highly Stretchable and Low-Voltage Wearable Heater. *Adv. Electron. Mater.* **2017**, *3* (9), 1700193. https://doi.org/10.1002/aelm.201700193.

(14) Sun, J.; Gong, L.; Lu, Y.; Wang, D.; Gong, Z.; Fan, M. Dual Functional PDMS Sponge SERS Substrate for the On-Site Detection of Pesticides Both on Fruit Surfaces and in Juice. *Analyst* **2018**, *143* (11), 2689–2695. https://doi.org/10.1039/C8AN00476E.

(15) Wang, Y.; Yu, Z.; Mao, G.; Liu, Y.; Liu, G.; Shang, J.; Qu, S.; Chen, Q.; Li, R.-W. Printable Liquid-Metal@PDMS Stretchable Heater with High Stretchability and Dynamic Stability for Wearable Thermotherapy. *Adv. Mater. Technol.* **2019**, *4* (2), 1800435. https://doi.org/10.1002/admt.201800435.

(16) Li, Y.-Q.; Zhu, W.-B.; Yu, X.-G.; Huang, P.; Fu, S.-Y.; Hu, N.; Liao, K. Multifunctional Wearable Device Based on Flexible and Conductive Carbon Sponge/Polydimethylsiloxane Composite. *ACS Appl. Mater. Interfaces* **2016**, *8* (48), 33189–33196. https://doi.org/10.1021/acsami.6b11196.

(17) Jang, N.-S.; Kim, K.-H.; Ha, S.-H.; Jung, S.-H.; Lee, H. M.; Kim, J.-M. Simple Approach to High-Performance Stretchable Heaters Based on Kirigami Patterning of Conductive Paper for Wearable Thermotherapy Applications. *ACS Appl. Mater. Interfaces* **2017**, *9* (23), 19612–19621. https://doi.org/10.1021/acsami.7b03474.

(18) Jiang, W.; Niu, D.; Liu, H.; Wang, C.; Zhao, T.; Yin, L.; Shi, Y.; Chen, B.; Ding, Y.; Lu, B. Robotics: Photoresponsive Soft-Robotic Platform: Biomimetic Fabrication and Remote Actuation (Adv. Funct. Mater. 48/2014). *Adv. Funct. Mater.* **2014**, *24* (48), 7597–7597. https://doi.org/10.1002/adfm.201470311.

(19) Yeo, J. C.; Yap, H. K.; Xi, W.; Wang, Z.; Yeow, C.-H.; Lim, C. T. Soft Robotics: Flexible and Stretchable Strain Sensing Actuator for Wearable Soft Robotic Applications (Adv. Mater. Technol. 3/2016). *Adv. Mater. Technol.* **2016**, *1* (3). https://doi.org/10.1002/admt.201670013.

(20) Hines, L.; Petersen, K.; Lum, G. Z.; Sitti, M. Soft Actuators for Small-Scale Robotics. *Adv. Mater.* **2017**, *29* (13), 1603483. https://doi.org/10.1002/adma.201603483.

(21) Lai, S.; Zhang, J.; Yan, Y.; Yu, H. Optimization Design Strategy of Electroadhesive Devices with Interdigital Electrodes Based on the Multiparameters Theoretical Model. *Math. Probl. Eng.* **2021**, *2021*, e3737490. https://doi.org/10.1155/2021/3737490.

(22) Argatov, I. I.; Borodich, F. M. A Macro Model for Electroadhesive Contact of a Soft Finger With a Touchscreen. *IEEE Trans. Haptics* **2020**, *13* (3), 504.

(23) Navas, E.; Fernández, R.; Sepúlveda, D.; Armada, M.; Gonzalez-de-Santos, P. Soft Grippers for Automatic Crop Harvesting: A Review. *Sensors* **2021**, *21* (8), 2689. https://doi.org/10.3390/s21082689.

(24) *Improving controllable adhesion on both rough and smooth surfaces with a hybrid electrostatic/gecko-like adhesive | Journal of The Royal Society Interface*. https://royalsocietypublishing.org/doi/10.1098/rsif.2013.1089 (accessed 2022-09-03).

(25) Guo, J.; Elgeneidy, K.; Xiang, C.; Lohse, N.; Justham, L.; Rossiter, J. Soft Pneumatic Grippers Embedded with Stretchable Electroadhesion. *Smart Mater. Struct.* **2018**, *27* (5), 055006. https://doi.org/10.1088/1361-665X/aab579.

(26) Mastrangelo, M.; Cacucciolo, V. High-Force Soft Grippers with Electroadhesion on Curved Objects; 2022. https://doi.org/10.1109/RoboSoft54090.2022.9762116.

(27) Asano, K.; Hatakeyama, F.; Yatsuzuka, K. Fundamental Study of an Electrostatic Chuck for Silicon Wafer Handling. *IEEE Trans. Ind. Appl.* **2002**, *38* (3), 840–845. https://doi.org/10.1109/TIA.2002.1003438.
(28) Eason, E. V.; Hawkes, E. W.; Windheim, M.; Christensen, D. L.; Libby, T.; Cutkosky, M. R. Stress Distribution and Contact Area Measurements of a Gecko Toe Using a High-Resolution Tactile Sensor. *Bioinspiration Ampmathsemicolon Biomim.* **2015**, *10* (1), 016013. https://doi.org/10.1088/1748-3190/10/1/016013.
(29) *Human climbing with efficiently scaled gecko-inspired dry adhesives | Journal of The Royal Society Interface*. https://royalsocietypublishing.org/doi/10.1098/rsif.2014.0675 (accessed 2022-09-03).
(30) Suresh, S. A.; Hajj-Ahmad, A.; Hawkes, E. W.; Cutkosky, M. R. Forcing the Issue: Testing Gecko-Inspired Adhesives. *J. R. Soc. Interface* **2021**, *18* (174), 20200730. https://doi.org/10.1098/rsif.2020.0730.
(31) *Ionic spiderwebs | Science Robotics*. https://www.science.org/doi/abs/10.1126/scirobotics.aaz5405 (accessed 2022-09-03).
(32) Prahlad, H.; Pelrine, R.; Stanford, S.; Marlow, J.; Kornbluh, R. Electroadhesive Robots—Wall Climbing Robots Enabled by a Novel, Robust, and Electrically Controllable Adhesion Technology. In *2008 IEEE International Conference on Robotics and Automation*; 2008; pp 3028–3033. https://doi.org/10.1109/ROBOT.2008.4543670.
(33) *An Electrostatic/Gecko-Inspired Adhesives Soft Robotic Gripper | Alizadehyazdi, Vahid; Bonthron, Michael; Spenko, Matthew | download*. https://ur.booksc.me/book/82675767/2af60b (accessed 2022-09-03).
(34) *Wall Climbing Robot Using Electrostatic Adhesion Force Generated by Flexible Interdigital Electrodes - Rong Liu, Rui Chen, Hua Shen, Rong Zhang, 2013*. https://journals.sagepub.com/doi/full/10.5772/54634 (accessed 2022-09-03).

CHAPTER 4

CONCLUSION AND FUTURE WORK

4.1 Overview

The present study demonstrates a novel method of patterning liquid metal on the soft substrates for its soft electronics. Thermoplastic poly(methyl methacrylate) (PMMA) was used to fabricate a mold using a commercial laser engraver (VLS 3.50, ULS) to define microchannels on the surface. The acrylic mold was then coated with FS using the sol-gel process to introduce the nanoscale roughness surface roughness to prevent the adhesion between the liquid metal oxide and mold surface. The study also promotes the use of other materials (beyond PMMA) to be coated with fumed silica for patterning the liquid metal geometries on the substrates. The acrylic mold has holes engraved on both ends of the microchannels. Liquid metal can be injected through these holes into the microchannels. The mold is then removed, leaving liquid metal on the substrate. The metallophobic FS coating prevents the metal from sticking to the mold. The patterned metal is potentially used as electrodes, sensors, wearable heaters, actuators, and soft grippers as discussed earlier.

4.2 Areas of advancement

A commercial laser writing system (VLS 3.50, universal laser system) using a 40 W CO_2 laser operating at 10.6 µm sanded the microchannels on the PMMA molds. The width of the geometries was restricted to 300 µm, but the main area for improvement in the liquid metal injection molding method for commercial printing of liquid metal would be to achieve higher

resolution. Therefore, improvement can be accomplished by engraving the microchannels with a higher resolution laser or other patterning techniques.

The liquid metal injection molding method has consistency and reliability for patterning different geometries of liquid metal on the substrates, Lifting the mold after liquid metal injection is a crucial step in maintaining consistent geometries, so work can be done to improve the controllability of this process. The challenges of applying pressure manually can be addressed in a better way during the manual injection printing of liquid metals. The present work demonstrates an advancement in continuous printing of liquid metal, which can enable commercial printing of liquid metal for its various applications in soft electronics. However, the process still needs to have a fully automated dispensing system for the injection of liquid metal through the microchannel mold. The system would ensure the specific volume of the liquid metal injected into the microchannels. The technology uses a piston to place the mold, which tends to apply uniform pressure and ensures clean removal of the mold, improving the consistency of the various patterns. The ability to print geometries on curved or non-flat surfaces is one of the most intriguing aspects of the current work because it allows for some of the most exciting applications for 3D-printed microelectronic devices. As a result, the use of LMIM in 3D-printed electronic devices can be explored in the future.

The work also reports the fabrication of a soft wearable heater for harnessing the Joule heating of the LM wires or geometries, The results and observation for a series of experiments indicated that the LM wire withstand the current density up to ~ 5 kA/cm^2 and beyond this value, the liquid metal line break or discontinues as shown in Figure 24(b).

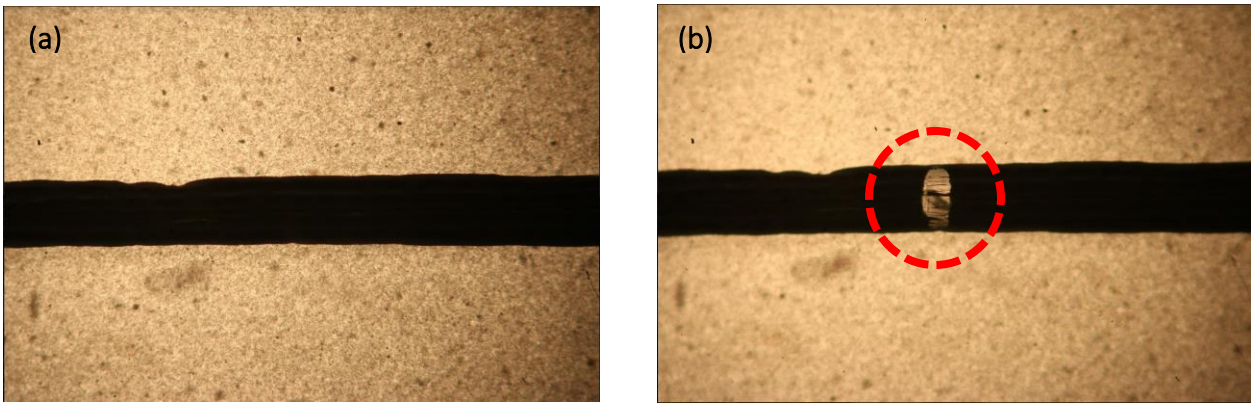

Figure 24: Microscopic image of LM wire encapsulated in elastomer (a) current density < 5 kA/cm^2 (b) current density >5 kA/cm^2

Future studies can investigate the cause behind the discontinuity of liquid metal wires at high current density. For example, it may be caused by thermal expansion differentials, or it could be caused by electromigration. The liquid metal wires were patterned and tested at high current values, and it was observed that the wire remains conductive for a current density less than 5 kA/cm^2 and beyond that the liquid metal discontinues as shown in Figure 24. Once they break, they no longer possess its electrical conductivity.

APPENDIX

EGaIn-Based Thermal Switch for Aerospace Applications

Dhwanil Vaghani, Omar Awartani, Michael Dickey

John P McHale, Payton J Batliner

The following is a technical report for a project I worked on during my MS thesis. The project focused on using continuous electrowetting to move slugs of liquid metal to enable thermal switching. We ultimately abandoned the project due to the formation of bubbles via electrochemical reactions that prevented the switch to be used in outer space applications.

ABSTRACT

Thermal management of satellites in orbit requires a careful balance of heat rejection to space via radiation with the internal and external heat loads. The thermal environment encountered by satellites varies greatly throughout the orbit which makes thermal management extremely difficult. One promising technology is a thermal switch which can provide thermal control by switching between high and low heat transfer regimes around a set point. The present research is carried out on passive techniques for the actuation of liquid metal by an electric field. The work primarily focuses on the continuous electrowetting of LM (CEW) in a confined operational condition for its application in thin thermal switches for space applications. The report briefly provides an overview of the research findings and attempts made to fabricate a fully operation thermal switch on a lab scale. It also provides brief insights into operational hurdles during the testing of the device and attempts made to resolve them.

EGAIN-BASED THERMAL SWITCH FOR AEROSPACE APPLICATIONS

Introduction

Thermal management of satellites is a primary requirement in recent times which requires a cautious balance of the heat rejection to space via radiation with the internal and external heat loads. The thermal environment encountered by satellites varies greatly throughout the orbit which makes thermal management extremely difficult. One promising technology is a thermal switch which can provide thermal control by switching between high and low heat transfer regimes around a set point. The ultimate need for thermal control has specifically become important with power densification resulting in devices with local heat fluxes as high as 1 KW/cm^2[1]. Primarily, the passive technique is explored more due to its reliability in the thermal expansion of the terminal material. Liquid metals are one of the most promising materials due to their unique duality of being fluidic and conductive at room temperature. Fundamentally, liquid metal has the property of forming a thin elastic oxide which is about the dimension of 3-5nm. The oxide help LM droplets to hold spherical shapes in ambient conditions. Gallium-based liquid metal LM is highly promising for its use in soft electronics due to lower vapor pressure and non-toxicity. Liquid metal possesses high thermal conductivity and relatively low conductivity. The property of LM of being actuated by an electric field has made it one of the potential materials for thermal management of the heat loads in satellites. The present research demonstrates the fabrication of the thin thermal switch harnessing the continuous electrowetting of LM. The report manifests challenges and outcomes for continuous electrowetting of liquid metal in a prefabricated acrylic geometry.

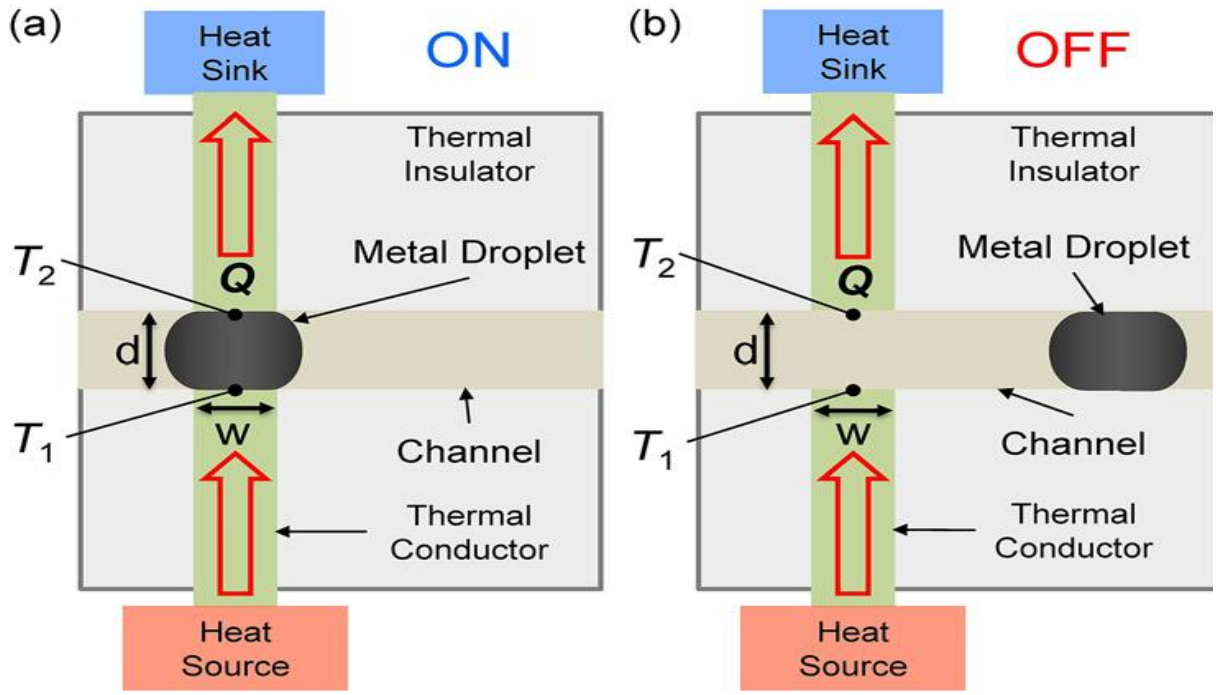

Figure 25: (a) "ON" state where LM droplet acts as a bridge for conduction of heat between source and sink. (b) "OFF' state where LM drop does not serves as a bridge between the heat sink and source[1].

The above-mentioned schematic demonstrates the actuation of LM droplets in a silicone channel filled with the reducing liquid or vapor which reduces the oxide formed and enables the motion within the channel path. The report will provide a brief overview of the experiments conducted for the fabrication of EGaIn-based thermal Switch applications for Space applications.

Purpose:

The previous work reported the continuous electrowetting of LM in a prefabricated "Master card shaped" switch filled with 1M NaOH (aq) as a fluid that keeps metal free from oxide. The device demonstrated was fabricated using a stack of acrylic pieces and was held un-sealed during the testing.

Methods and materials

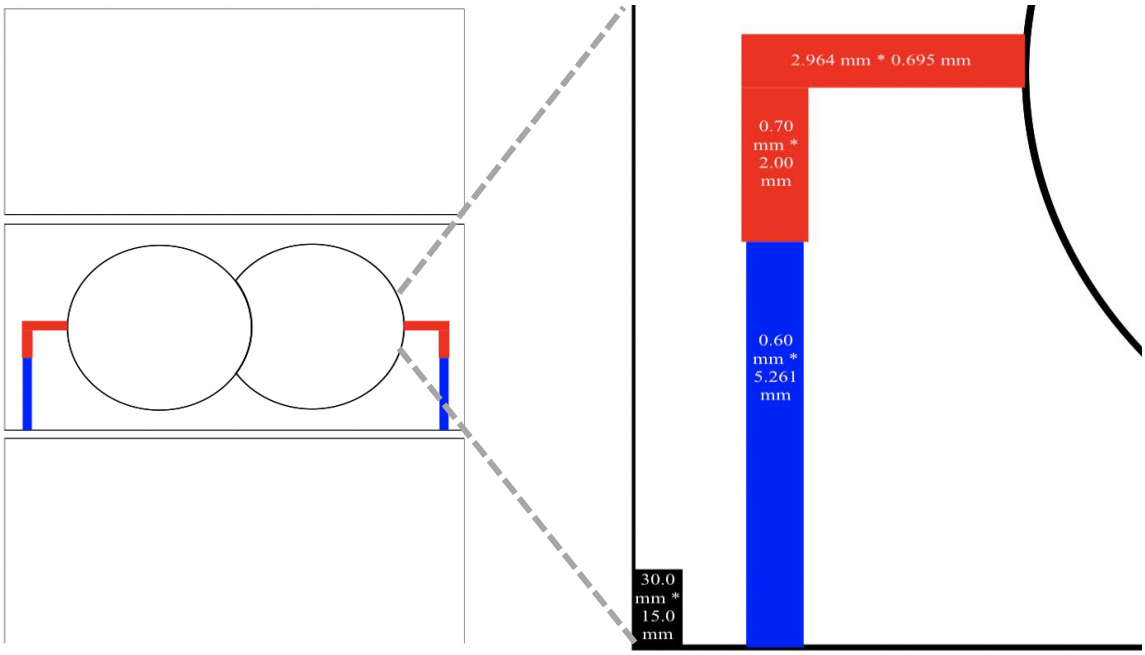

Figure 26: (a) Top-down schematic of the thermal switch "Master card design". The blue/red region houses the electrodes. The liquid metal will reside in the round regions and move back and forth between the two round chambers via continuous electrowetting. (b) Dimensions of the channel used for connecting electrodes.

The work has demonstrated the continuous electrowetting of liquid metal in the master card design for controlled motion of LM for thermal switch applications. The master card design was intended to have two chambers and of them would serve as a thermally conductive path when LM gets displaced to act as a bridge between the heat source and heat sink (Which reside below and above the disc-shaped chamber). The initial design and fabrication were done with PMMA (acrylic of thickness 2mm). The dimensions of the channels were estimated by trial and error and the depth of these channels was measured by Laplace pressure difference equations. The work demonstrated the use of AC Square wave signals for the CEW of EGaIn.

Table 2: Function wave generator parameters

Signal	Frequency (Hz)	Amplitude (Vpp)	Offset (DC)	Duty Cycle (%)
Ac square wave	**1 µHz**	**1**	**± 4.5**	**80**
Ac square wave	**1 Hz**	**1**	**± 4.5**	**80**

Ac square wave	**10 Hz**	**1**	**± 4.5**	**80**
Ac square wave	**50 Hz**	**1**	**± 4.5**	**80**

Observation:

The testing was carried out with a square wave of variable frequency and the above-mentioned parameters. The work shows pulsation at frequencies of 1 Hz, 1 Hz, and 10 Hz, however, it begins to decline when the frequency is increased while the time for completing each cycle decreases. For each cycle, the signal is in the positive phase for 80% of the time and in the negative phase for 20% of the time. The device that was tested with these parameters allows for continuous electrowetting of LM, and the LM slug displaces the reducing liquid in either chamber, depending on the polarity of the applied voltage. The signal tends to behave like a DC signal when the frequency value increases and hence the pulsation of LM is not evident during normal observation. The existing work done by the team was reviewed and few key issues were found, and future work was proposed to address the problems.

Key issues and future work

The testing of devices manifests the CEW of LM slug inside the device which can potentially use for managing the heat loads of the satellite.

1. **Robust sealing**

Since the device is unsealed the reducing fluid (NaOH) was displaced and pumped out through the electrode channels and over time after a few cycles the device is just left with LM slug and air which results in oxide formation and hence ultimately hinders the motion and CEW. This section will address the issue of sealing and prospective solutions to avoid the leakage of reducing fluid from the device.

2. **Electrolysis**

The reducing liquid is aqueous NaOH and hence one of the major problems observed using the aqueous solution in a confined device with the voltage value mentioned earlier results in the electrolysis of water which enables the formation of H_2 and O_2 gases at the respective electrodes. These gases in form of air bubbles not only disrupt the contact between electrolyte and electrodes but also form oxide around the LM slug which leads to adhesion of the oxide with the acrylic (top and bottom substrates). The reports manifest the work done to solve the problem of electrolysis and eliminate the bubbles formed to an extent that will guide the future direction of the project.

3. **Redefined geometries**

Since the voltage value required to enable CEW of LM slug in master card design was higher than the electrochemical windows (1.23 eV). The bubbles were introduced to the system by electrolysis of water and hence the report demonstrates the work done to design and test geometries other than master card design for the lower voltage drop across the path.

4. **Reaction of EGaIn with (NaOH)**

The formation of bubbles was also suspected as a byproduct of the reaction between the EGaIn and NaOH and hence several attempts were made to define an alternative reducing liquid instead of NaOH. The report manifests the work done on various electrolytes to enable CEW of LM slug in a confined device.

1. ROBUST SEALING

Purpose

The voltage-driven CEW of liquid metal slug in the reducing liquid media (NaOH) causes pumped of the low viscous/denser fluid out through the microfluidic channels designed for the electrodes and this causes air to enter the device that results in the formation of oxide causing the device to stop functioning. The aim here is to apply a robust sealing that avoids the leakage of NaOH from the device and prevents the air from entering to the device.

Proposed solution

The device is sealed with robust sealing by using the scotch-weld 2216 B/A (5:7) and Epoxy (353 ND) A: B (1:10). The epoxy takes around 24 hours for curing under ambient conditions, while takes around 3-4 h. when kept in an oven at 80 C. The sealing was robust enough to avoid any sort of leakage from adjoining points of three acrylic pieces.

Method/ Process/ Experimentation

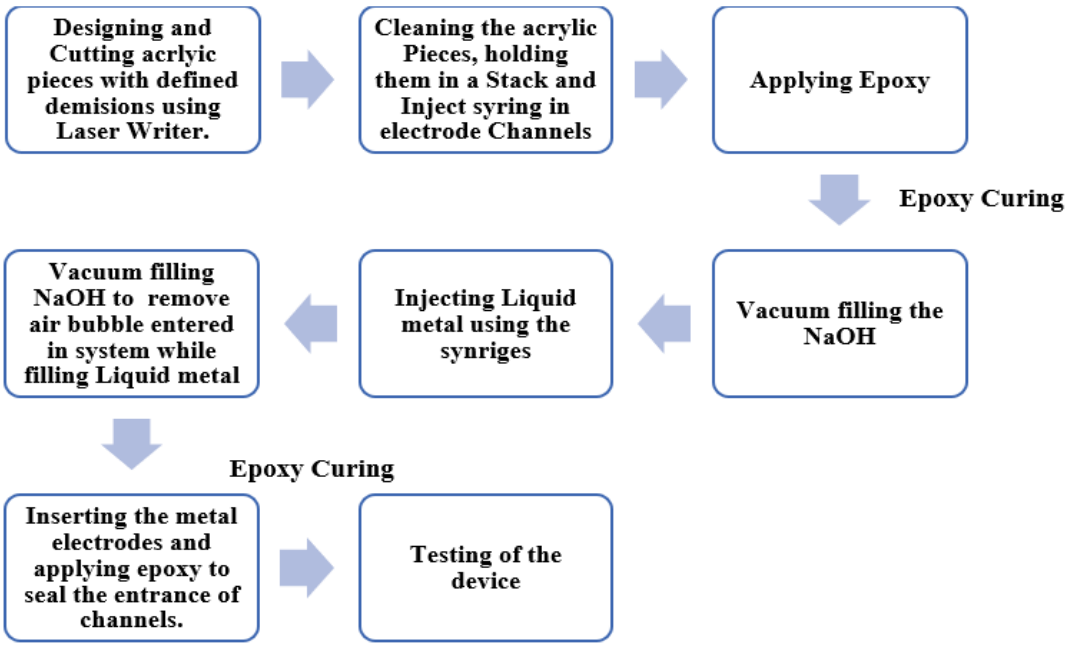

Figure 27: Existing process flow for fabrication of thin thermal switch

The above-mentioned process flow has been used for the fabrication and testing of the thin thermal switch. The sealing of the device was found to have certain flaws and due to which an additional step was defined to enhance the adhesion between different acrylic pieces.

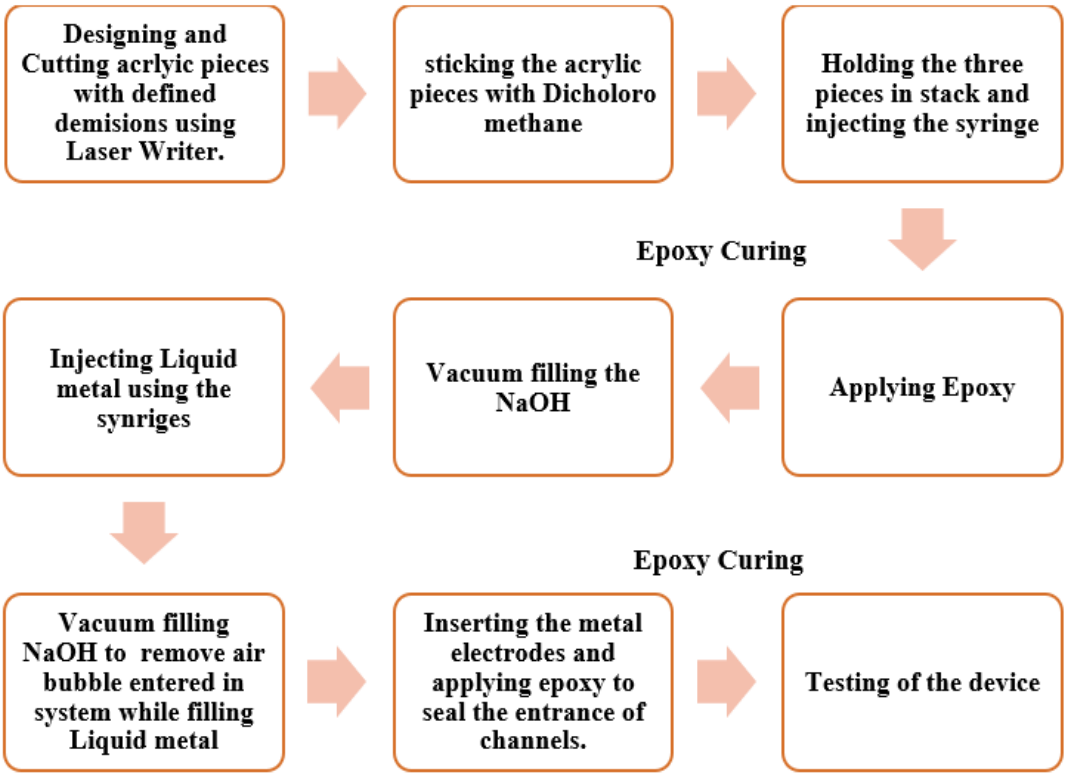

Figure 28: Modified process flow for fabrication of thin thermal switch

Observations

The sealing of the device proved to prevent major leaking of the reducing fluid during a test of the device. The viscosity of the epoxy is relatively less and due to this, the epoxy flows through the gaps between the acrylic pieces leading to channel clogging and hence the electrode channels get blocked.

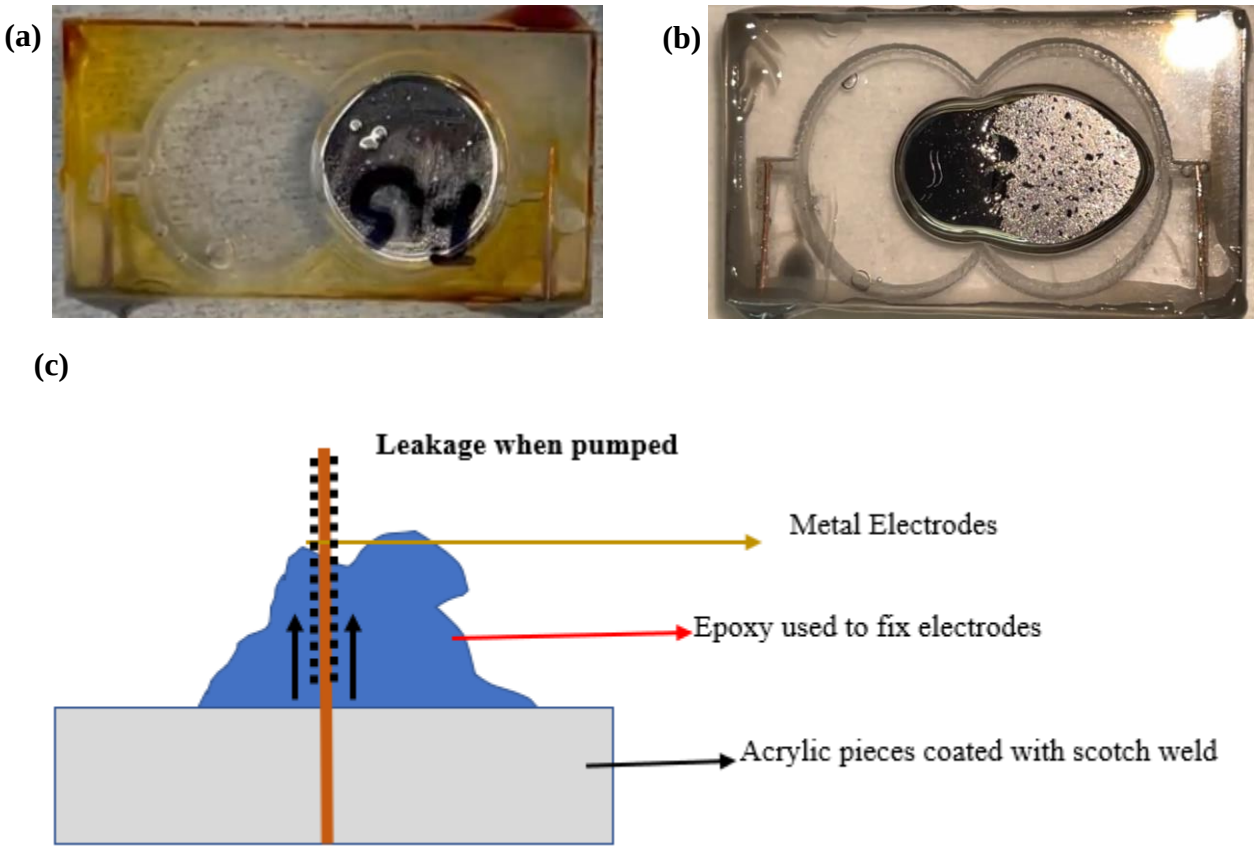

Figure 29: (a) Master card design sealed with the epoxy (b) Master card design sealed with scotch weld (c) Schematic showing leakage of electrolyte due to poor contact of scotch weld with a metal electrode

Figure 6 (a & b) demonstrates the sealing of the device using scotch weld and epoxy. The work reports that the adhesion of metal electrodes with the epoxy and scotch weld is poor due to which there is often a chance of leakage of NaOH through the electrode channel as shown in Figure 6 (c). This also leads to evaporation of the electrolyte at required conditions.

Outcomes

The later experiments can be done using some glue or epoxy which makes good contact between the metal electrodes. Torr Seal and silicone are suggested to be used for the better sealing of the electrode channels.

2. ELECTROLYSIS

When the voltage value is applied beyond the electrochemical window (1.23 eV), the aqueous reducing liquid employed as an electrolyte undergoes electrolysis leading to hydrogen and oxygen gas evolution. According to previous research, the minimum offset voltage necessary for enabling the CEW of the LM slug in master card design is 4.5 V, which is higher than the electrochemical limit, resulting in the evolution of H_2 and O_2 gas at corresponding electrodes. Over numerous cycles of the LM slug moving on either side (chamber), these air bubbles grow large enough to create an oxide around the slug, resulting in oxide adhesion to the substrate (Top and Bottom pieces or layer).

Purpose To eliminate or suppress the formation of air bubbles for increasing the shelf life of the device.

Method/ Process/ Experimentation

a) Electrode materials

To resolve the formation of bubbles various metallic electrodes were tested to suppress or eliminate the formation of bubbles including copper, nickel, platinum, and tungsten.

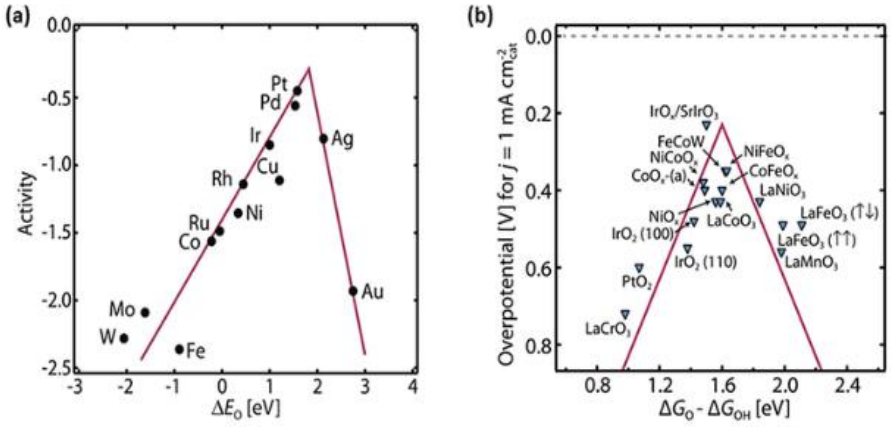

Figure 30: (a) OER volcano plot for metal (b) OER volcano plot for metal oxide

The above Figure demonstrates the voltage value for oxygen evolution reactions for different metal and metal oxide. It was found that with a combination of metal as cathode and anode, the HER and OER intensify, and the device quickly gets to the point where it stops functioning further. The threshold voltage value required for the CEW of LM is beyond the initiation of hydrogen or oxygen evolution reactions and hence it is extremely difficult to suppress the formation of the bubbles with different metal and metal oxide electrodes. The experiments were conducted with copper, nickel, and platinum electrodes, copper was observed to get errored over time due to its reactivity with the electrolyte while nickel and platinum do not chemically react with the electrolyte. However, the work can be done for advanced research on hybrid metallic alloy electrodes which also are prone to react with the reducing liquid (NaOH), but the present work was limited to the use of traditional metal electrodes for the continuous electrowetting of LM.

b) Electrolytes

Another possible way of suppressing or reducing the formation of bubbles inside the system was to find an alternative to the reducing liquid or electrolyte. The present work focuses more on finding the optimum concentration of aqueous NaOH to reduce the formation of bubbles and increase the shelf life of the device. Subsequently, an alternative electrolyte was worked upon to serve the purpose of continuous electrowetting of liquid metal in confined geometry.

Purpose To find an alternative composition of electrolytes that suppresses or reduces the intensity of bubbles formed during the function of the device.

Method/ Process/ Experimentation

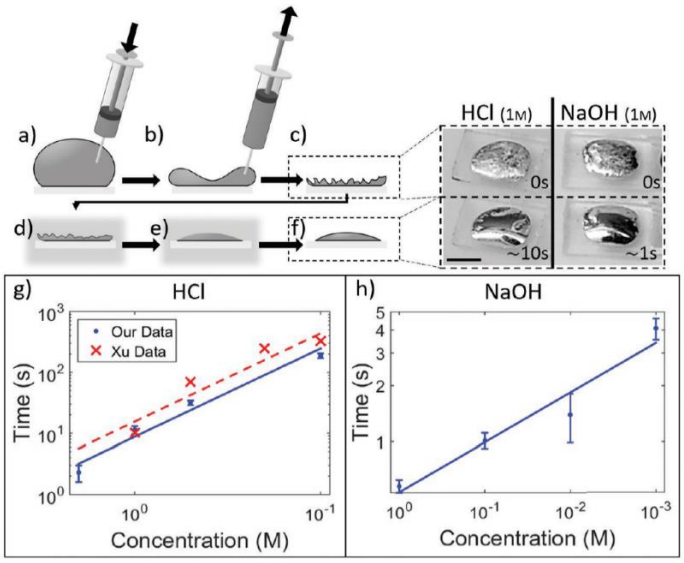

Figure 31: Time vs concentration of acid or base for removal of oxide [4].

The above Figure demonstrates the time vs concertation of the reducing liquid used to get rid of the oxide. The initial trials were made by reducing the concentration of NaOH starting with ranging from 0.01 M to 1 M.

Table 3: Observations at different concentrations of NaOH

NAOH CONCENTRATION (M)	DID EGAIN MOVE?	BUBBLE FORMATION	OXIDE FORMATION (OVERNIGHT)
0.01	No, EGaIn Didn't move at a voltage range from 1V to 4.5V	Yes, but fewer bubbles were observed	Yes
0.05	Yes, EGaIn moves with V>3 V	Yes, but fewer bubbles were observed	Yes

0.1	Yes, EGaIn moves with V>3 V	Yes, but fewer bubbles were observed	Yes
0.125	Yes, EGaIn moves with V>3 V	Yes, but fewer bubbles were observed	Yes
0.25	Yes, EGaIn moves with V>3 V	Yes	No
0.5	Yes, EGaIn moves with V>3 V	Yes	No

The results suggested with the decrease in the concentration of NaOH, the intensity of bubble formation was reduced and therefore the shelf life was increased but bubbles were still not eliminated from the system. The conductivity of the solution decreases with the decrease in the concentration of NaOH and hence other salts were tested to increase the conductivity of the electrolyte. Buffers such as $NaNO_3$, NaH_2PO_4, and Na_2SO_4 were ineffective in preventing bubble formation at the electrodes and did not seem to slow down the electrolysis.

Therefore, further advancement of the work was pursued for finding an alternate electrolyte with ideal characteristics that enable CEW of LM in a confined (sealed) device without any formation of bubbles and erosion of electrodes. The two pathways for finding electrolytes involves aqueous and non-aqueous electrolyte. The work on aqueous electrolytes was proposed for increasing the range of the e-chem window to avoid electrolysis at lower voltage values. Primarily for the selection of the ideal electrolyte, the following criteria need to be addressed.

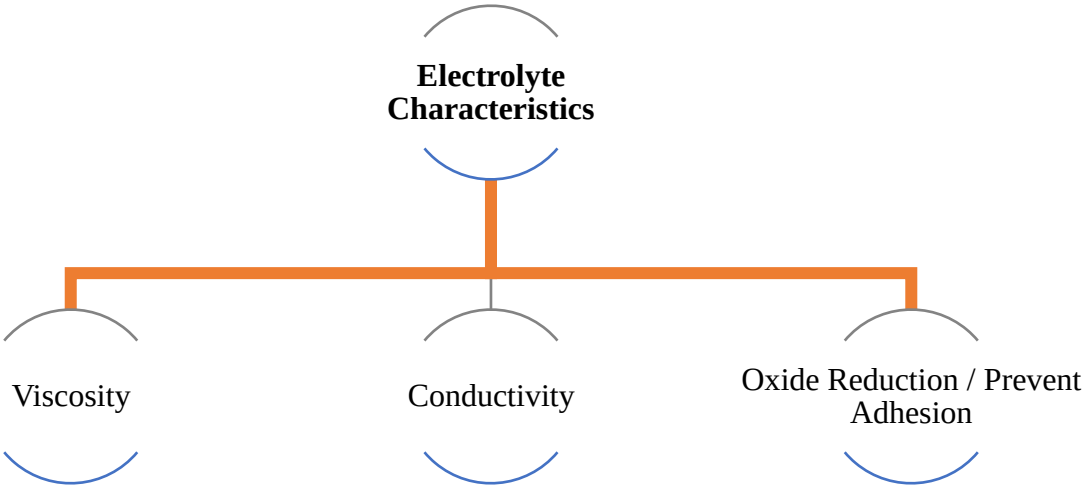

Figure 32: Electrolyte characteristics

- The viscosity of the electrolyte should be less than the viscosity of the LM slug.
- The electrolyte should be conductivity.
- The electrolyte should be sufficient to reduce the oxide around the LM slug to avoid any sort of adhesion.

1-decylphosphonic acid (DPA) ethanolic solution

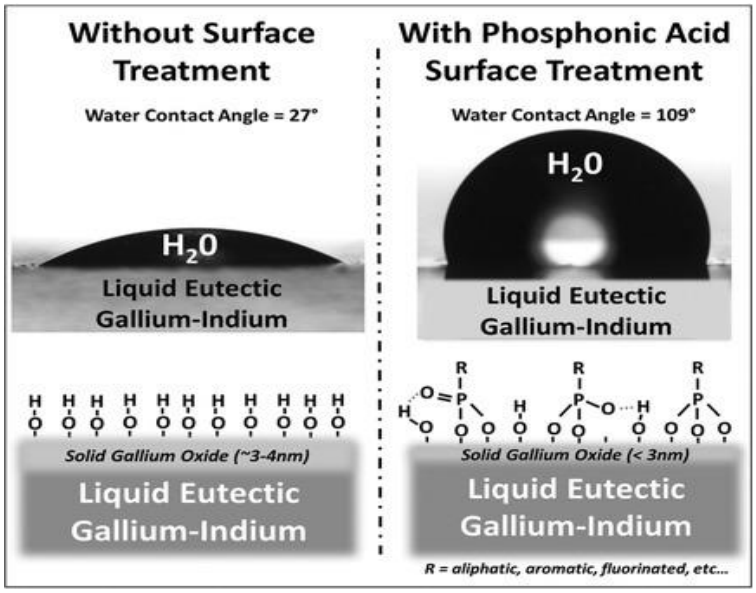

Figure 33: Surface treatment for increasing the contact angle [2]

Phosphonic acid modifiers are used to modify the fluid interface chemistry rather than removing the oxide. The phosphate group favors the adsorption of metal oxide through several bonding including hydrogen and some covalent bonds. Phosphonic acid treatments result in the formation of low surface energy hydrophobic surface which eliminates adhesion of the oxide skin to substrates while simultaneously controlling the thickness of the native surface oxide.

Non-aqueous electrolyte

2 M NaOH in Methanol (MeOH)

Previous work has reported the use of 2M NaOH being effective in keeping the LM drops oxide free. The present work replicates the use of 2M NaOH for the CEW of the LM. The electrolyte has also been to reduce the oxide layer and avoids LM to adhere with substrates. The mentioned electrolyte however tends to reflect precipitation and settling of NaOH particles which can break the contact of the electrode with the electrolyte in the longer run. Bubbles were observed on the application of the threshold voltage for continuous electrowetting of liquid metal. The gas evolved can be carbon dioxide, hydrogen, methane, etc.

0.2 M Tetrabutylammonium chloride in acetonitrile

The organic solvent (Acetonitrile) was employed in the experiment; however, it lacked conductivity. So, tetrabutylammonium chloride in acetonitrile was used as salts to provide free ions and improve conductivity. There were no bubbles found when voltage was applied through acetonitrile without salts, whereas the electrolyte with salts initially removes the oxide when voltage is applied, but as the voltage is increased, bubbles appear in the system, ruling out the use of electrolyte for CEW of LM in thermal switches.

3. REDEFINING THE GEOMETRIES

The continuous electrowetting of LM in master card design requires a threshold value of about 4.5 eV for the complete functioning of the device. The voltage required is higher than the electrochemical window and hence to avoid the generation of bubbles, some changes were made in the design to lower the voltage drop.

Purpose To lower the voltage value for CEW of LM to eliminate the formation of the bubble via electrolysis of the aqueous electrolyte (NaOH)

Method/ Process/ Experimentation

The initial experiments were designed to reduce the voltage value required for CEW of LM by decreasing the width of the channel and correspondingly reducing the volume of LM slug in the device

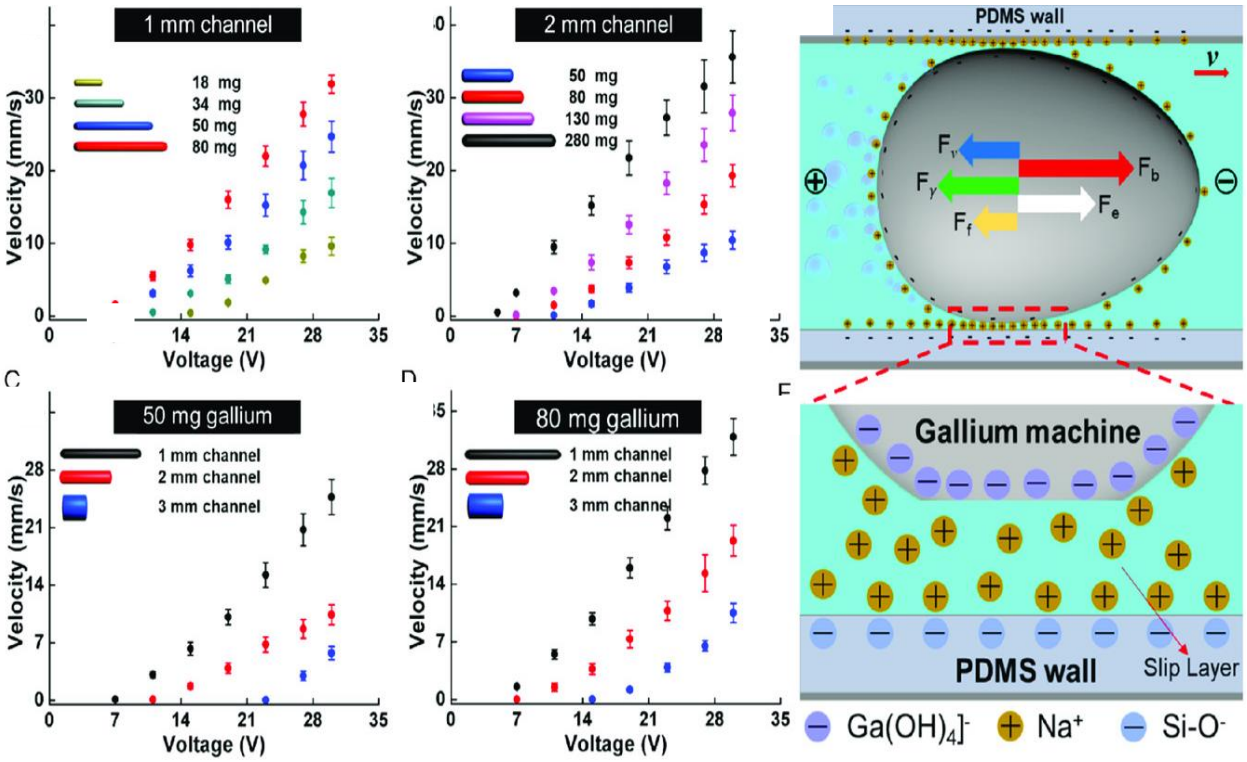

Figure 34: Relationship between velocity, voltage, and channel width [3]

The above Figure demonstrates the relation between the width of the channel and the voltage value required for different volumes of the LM slug in the device. The relation shows the voltage value required for CEW of LM increases with the increase in width of the channel and the volume of the LM in the device. Hence, few attempts were made to narrow down the channel width to reduce the voltage value.

A) Adding a shelf to the master card design

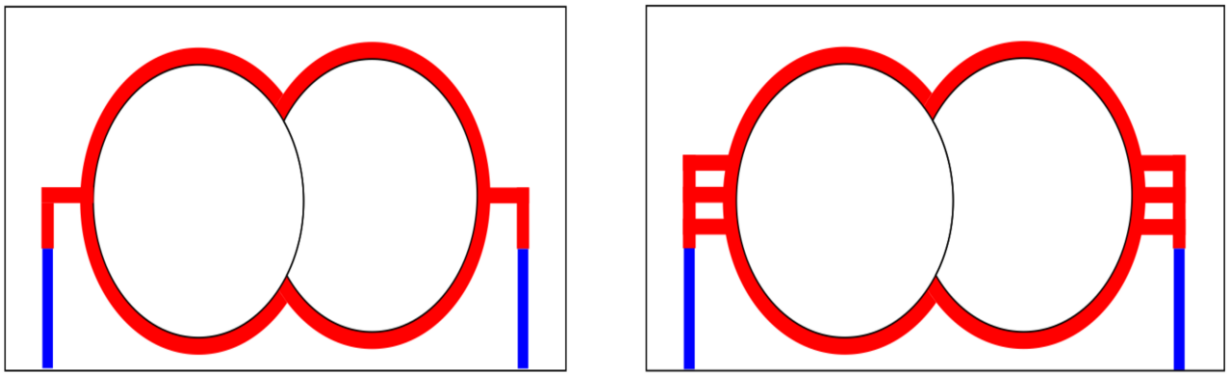

Figure 35: Schematic for master card design with shelf

The shelf was added for bubbles to have an escape route to avoid any sort of hindrance for the LM slug to have transitioned from one side to another. The notion was to add excess NaOH to increase the shelf life and decrease the voltage value. The second design was proposed to enhance the contact between the electrolyte and electrode and was thought to increase the life of the device.

Observations: The experiments conducting a design test yields no significant drop in the value of voltage required for the CEW of LM. The shelf however served the purpose for air bubbles to escape and reduces the hindrance to the transition of LM, but the voltage required was about the same.

B) Circular design

The attempts were made to design a circular geometry for the Thermal switch device. This involves multiple electrode designs for better controlling the motion of the LM slug in the NaOH.

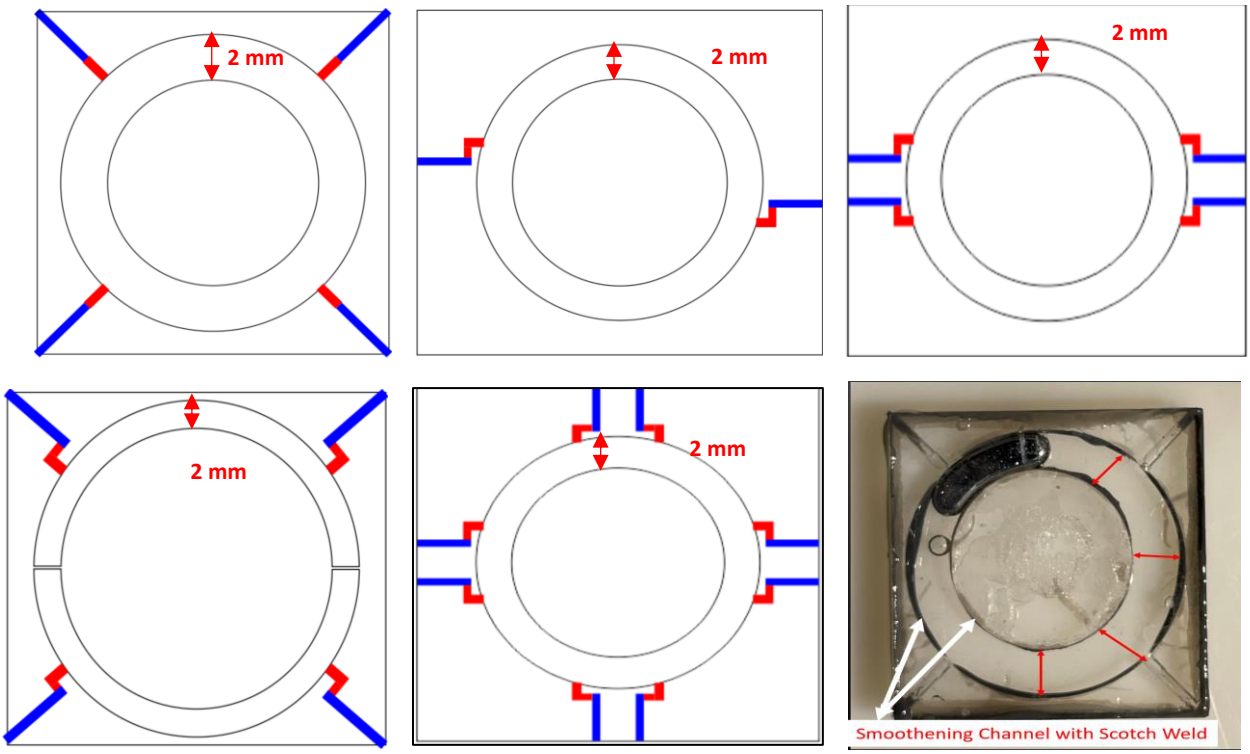

Figure 36: Schematic for circular design

Observations

The circular channels with multiple electrodes were designed for the CEW of LM. The design was made with the prospects of having better controllability and lowering the voltage value to avoid electrolysis of the reducing aqueous NaOH.

There were difficulties with the manual fabrication of these circular geometries due to their design the top, bottom, and central layers were hard to be placed in stack symmetrically. The laser cuts the acrylics thoroughly and therefore makes it difficult to have a uniform channel width with the center part being stuck manually with epoxy. The initial design shown in the Figure has a

straight electrode channel which causes the leakage of NaOH and hence the geometries of the electrode channels were re-defined to avoid leakage of the electrolyte. The devices were then tested with lower voltage values and in the initial reading, the LM slug was found to be triggering or vibrating about its place. However, the motion was not controllable. The device was further found to have leakage issues to manual sealing and stop functioning after a few testing attempts. Short-circuiting of the device was also an issue hampering the controlled continuous electrowetting of liquid metal. The minimum voltage value used for the motion of LM was 2.5 V but again it was not stable and may the potential reason can be shorting of the device.

C) Semicircular design

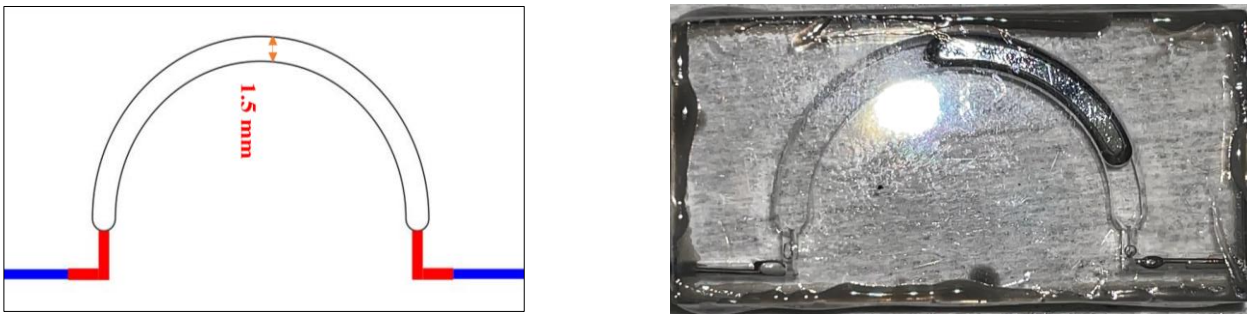

Figure 37: Schematic for semi-circular design

Table 4: Testing parameters for semi-circular design

Signal	AC Square Wave
Solvent	0.05 M NaOH
Design	Semi-circular
Channel Width	3 mm
Frequency	10 mHz
Amplitude	1.20 Vpp
Offset	0 VDC

Duty Cycle	50 %
Electrode	Ni (2)

The semi-circular designs seem to be promising in the initial testing but later the device stops functioning after a few cycles. The potential reasons were the formation of oxide, leakage of the electrolyte, etc. The insufficient quantity of the electrolyte can also be a cause for the formation of oxide as there is always some leakage of electrolyte due to a lack of robustness in sealing.

D) Straight channel designs

The straight channel was designed to conduct a trial and error-based experiments to find the threshold voltage required to enable continuous electrowetting of LM for its application for space application.

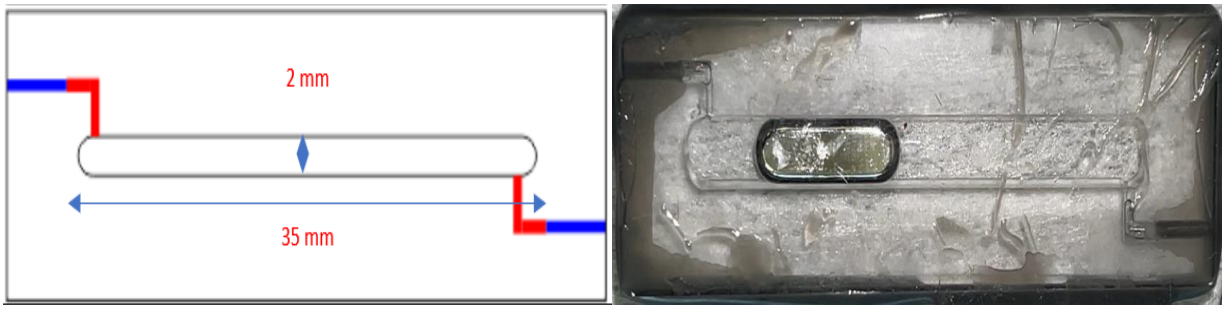

Figure 38: Straight channel design

The single channel geometries were tested and the following are the threshold parameter observed for enabling continuous electrowetting of LM.

Table 5: Testing parameters for straight channel design

Signal	Frequency (Hz)	Amplitude (Vpp)	Offset (DC)	Duty Cycle (%)
Ac Square wave	**100 mHz**	**1.2**	**0 VDC**	**50**

Multiple parallel channels

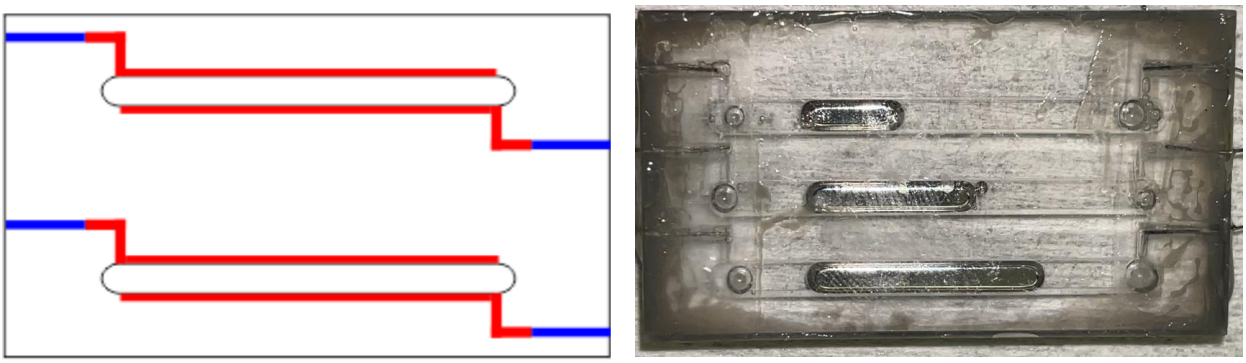

Figure 39: Multiple parallel lines

The multiple channels were tested with different volumes of liquid metal for finding the combination that works best, which is also mentioned earlier. The channel with a higher volume of LM tends to move faster compared to the channel with a lesser volume, as it moves to the other end. This may be because with a larger volume of LM in the channel the path or distance that needs to reach the other end is less and hence it covers up faster than the channel with less volume of LM. The following was the parameter used for the testing.

Table 6: Testing parameters for multiple parallel lines

Signal	Frequency (Hz)	Amplitude (Vpp)	Offset (DC)	Duty Cycle (%)
Ac Square wave	**100 mHz**	**1.2**	**0 VDC**	**50**

The device works well for the initial few cycles but then it tends to get adhere to the acrylic substrates and ultimately stops functioning in the longer run. The key observation here device when tested after 24 h. after its fabrication, the above-mentioned parameter didn't work. The possible cause for this is the formation of oxide as the device is untested for 24 h, LM slug forms oxide and adheres to the substrates which then makes it difficult to enable CEW with a lower voltage value.

Fumed silica coating

The proposed solution for preventing the oxide adhesion with the acrylic substrates can be introducing some roughness which is reported to prevent the adhesion of oxide by the previous work done in the Dickey Group. The nano-particle coating introduces nano-scale roughness around 1-10 nm depending upon the exposure time. The FS physically absorbs to the surface of acrylic (PMMA) by plasticization making the surface tacky which makes the surface have poor contact with the LM oxide.

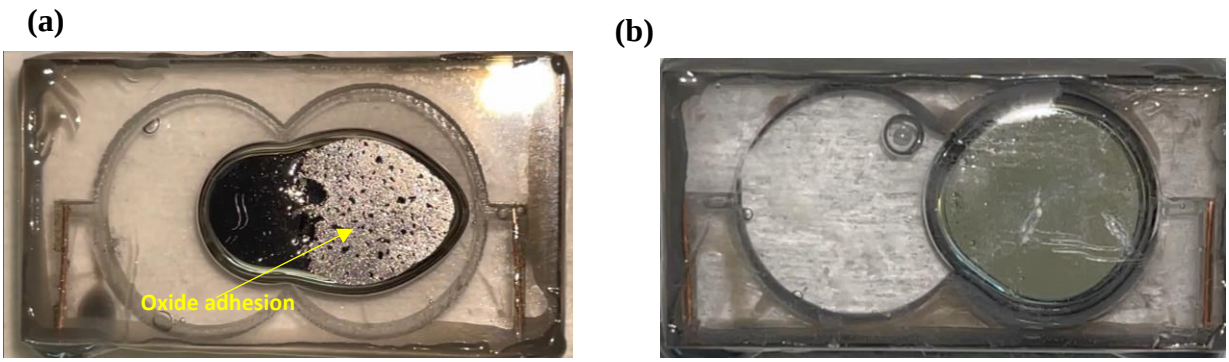

Figure 40: (a) Oxide adhesion on uncoated PMMA substrate (b) Fumed silica coated PMMA

E) Reservoir design

The purpose of designing the device with a reservoir was to have an excess electrolyte to avoid the formation of oxide and enable the smooth function of the device for a longer period. The single channel design was modified, and some modifications were made to the sealing process.

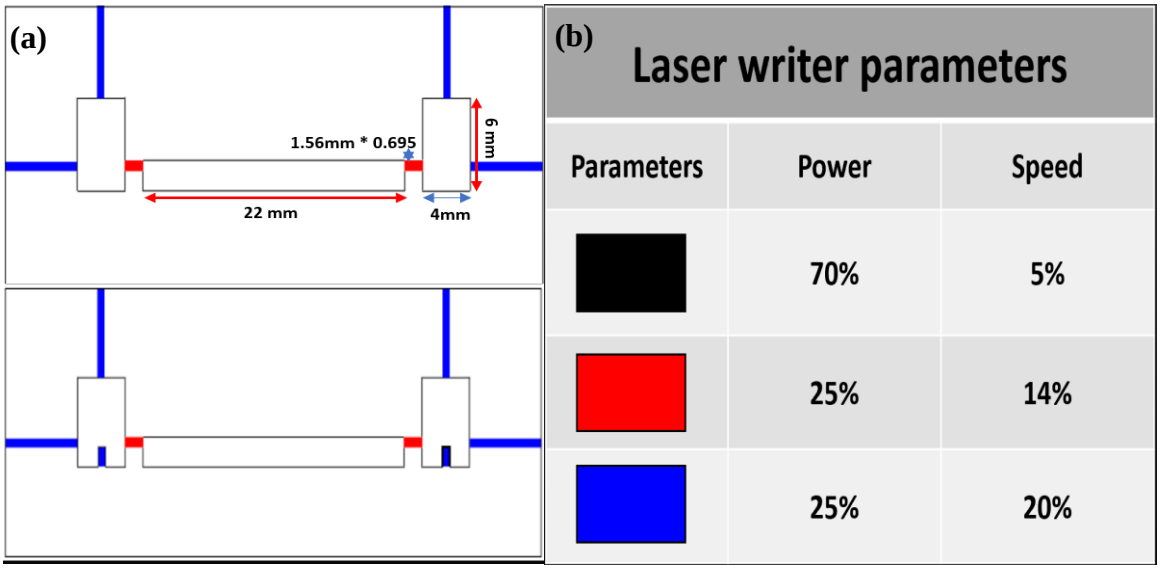

Figure 41: (a) Reservoir design (b) Laser writer parameter

The Figures manifest the single channel design with two reservoirs of excess NaOH. The device was made by cutting the PMMA with mentioned laser parameters. The device was sealed with slight modification in the procedure, the below-mentioned chart is the procedure adopted for the fabrication of the device.

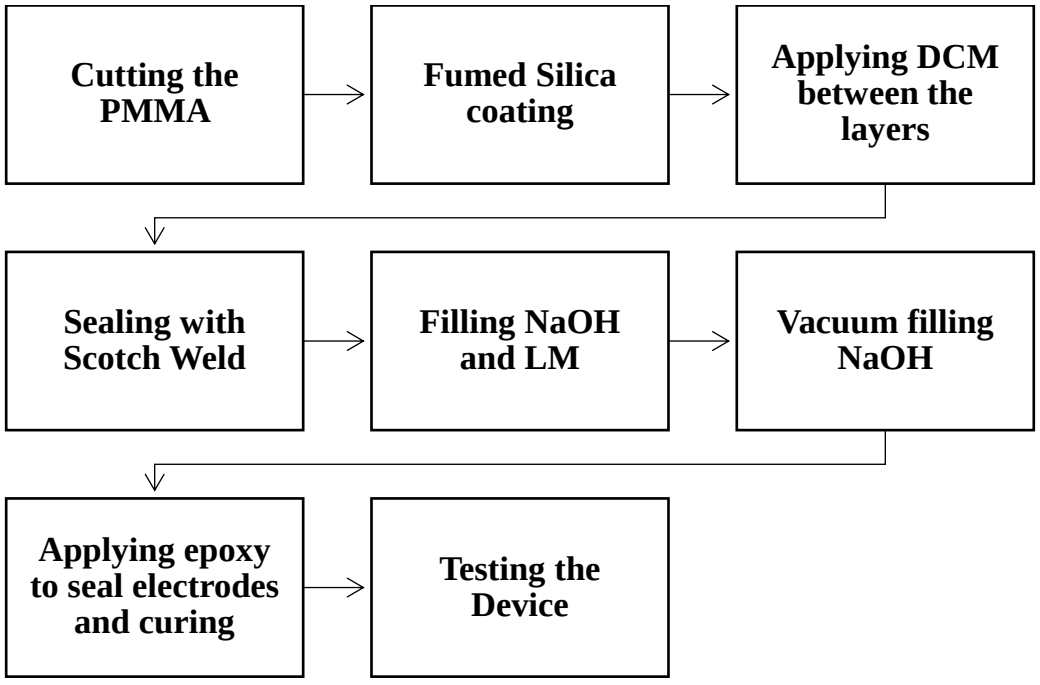

Figure 42: Process flow for fabrication of the device

The device was tested using AC square wave signals and DC voltage to determine the value of the threshold voltage enabling the CEW of LM for the thermal switch. The experiments were conducted continuously for the AC square signals while for DC signals the tests were made in regular time intervals.

AC Square signals

Table 7: Parameters for testing reservoir design

Signal	Frequency (Hz)	Amplitude (Vpp)	Offset (DC)	Duty Cycle (%)
Ac Square wave	**100 mHz**	**2.3**	**0**	**50**
Ac Square wave	**5 Hz**	**1.2**	**0**	**80/20**

The first configuration was used to have continuous testing of the device and determine its life of the device. The latter configuration was used to test the device on time-based intervals with a difference of 24 h for a week.

(a) **(b)**

Figure 43: Reservoir design (a) at 0 h (b) after 144 h

The device was tested using the first configuration continuously overnight for a week. Figure (a) shows the fabricated device after curing and the device shown in Figure (b) is after 144 h. from the beginning of the test. The formation of bubbles was gradual over time but significant enough to get into the path of LM in the channel and block the motion. The device worked well for a week before it stops functioning. The latter configuration was used for testing the device at regular intervals and it worked well for 12 days. The LM slug forms oxide and gets adhered to the wall of the channels as it is on rest for 24 h. between two testings.

DC Voltage bias

Table 8: DC voltage parameters

Signal	Frequency (Hz)	Amplitude (Vpp)	Offset (DC)	Duty Cycle (%)
DC Signal	**-**	**-**	**1.2**	**-**

The device was tested using DC voltage, and it was initially noted that the device operated properly for the mentioned voltage value at regular intervals.

(a) **(b)**

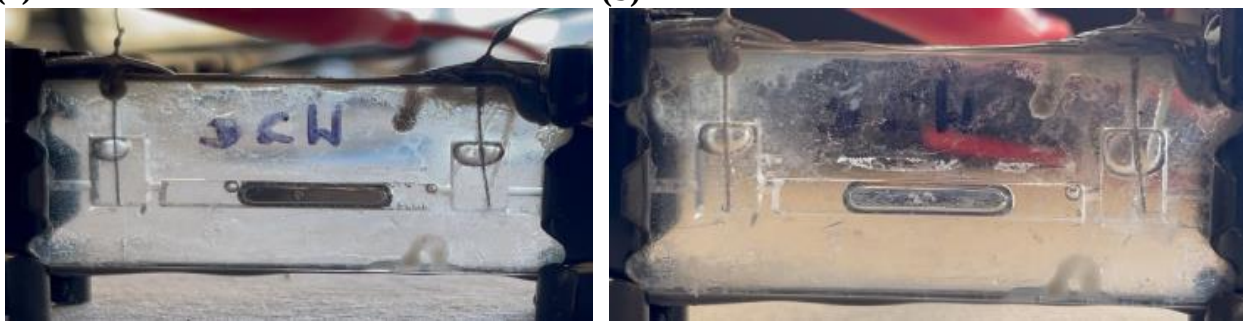

Figure 44: Reservoir design (a) at 0 h (b) after 120 h

Figure 20 (a) demonstrates the initial testing after the fabrication of the device, there are some bubbles in the system before the testing. These bubbles may have been introduced into the system during the injection of LM by the pressure difference created with injection and ejection of the syringe into the channels. The curing of the epoxy used to plug the channels' exit holes is another potential reason why these bubbles could enter the system.

4. Reaction of EGaIn with NaOH and Water

Purpose

To investigate the presence of a bubble in the sealed device.

Method/ Process/ Experimentation

The device was tested at a DC voltage of 1.2 V, which is below the electrochemical window for aqueous electrolyte electrolysis. Experiments were carried out by creating a device filled with LM and electrolytes without any electrodes to investigate the reasons for the presence of bubbles in a confined or sealed device.

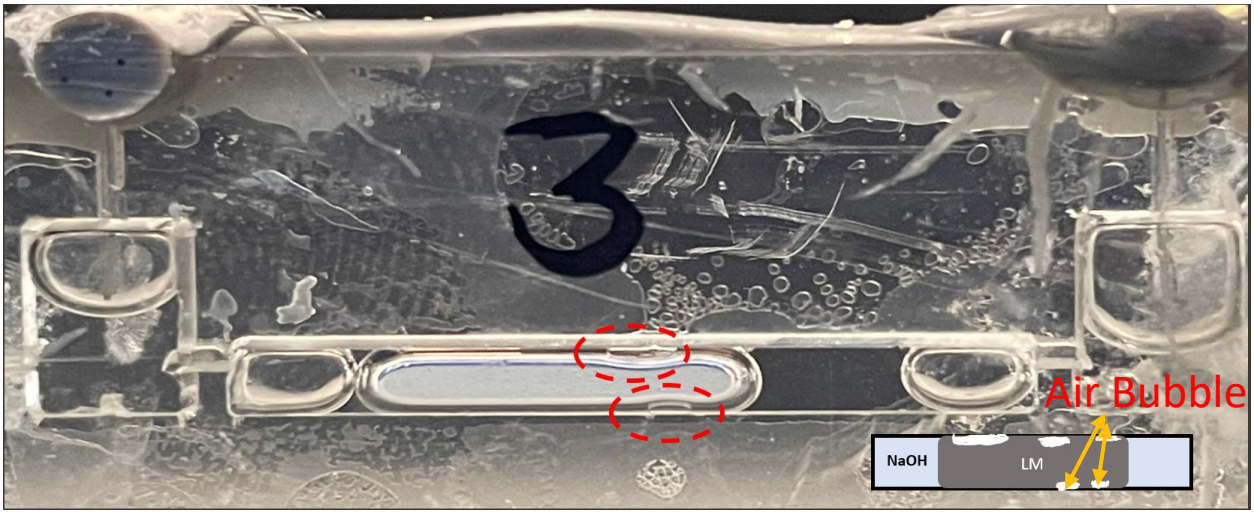

Figure 45: Bubbles formed by the reaction of LM and electrolyte

A commercially available scotch weld was used to completely seal the device, which was then monitored for roughly 10 days. This was never meant to evaluate the device for CEW of LM. Thus, the theory of electrolysis-induced bubble formation was terminated. As a result of the

mentioned fabrication issues, the gadget does have some bubbles in the reservoir. Even though the device was kept idle function any motion, the bubbles keep enhancing the device. As shown in the Figure after careful observation, some bubbles were found to be on the peripheral region between LM slug and channel walls which leads to the formation of oxide and ultimately hinders the motion of LM. The potential reason for it is a reaction between the LM and electrolyte i.e., NaOH.

$$2Ga + 2NaOH + 6H_2O \rightarrow 2Na[Ga(OH)_4] + 3H_2$$

This was also verified by a simple experiment of Injecting a few drops of LM and adding NaOH to it in the vail and sealing it. The vial was kept idle for a few days and was monitored.

(a) **(b)**

Figure 46: Vial experiments (a, b) bubbles formed by the reaction of LM and 1 M NaOH electrolyte

Initially, there were small air bubbles present on the LM slug which keep enhancing over the next few days and ultimately get combined to form a bug air bubble as shown in Figure (b).

Prospects

The current methods used to build systems that are susceptible to air bubbles are insufficient and can be improved as the research objective is to fabricate a device with absolute eradication of bubbles inside the sealed system. However, research finding demonstrates various issues that need to be addressed to make the system bubble free for its use in thermal space applications. Future work can be done to synthesize an alternative electrolyte that is conductive, chemical non-reactive, less viscous, and has characteristics to reduce the LM oxide. The CEW of LM in a sealed device provides great controllability for thermal switch application by tuning the voltage, frequency, and duty cycle parameters.

Reference

(1) T. Yang, B. Kwon, P. B. Weisensee, J. G. Kang, X. Li, P. V. Braun, N. Miljkovic, W. P. King, "Millimeter-Scale Liquid Metal Droplet Thermal Switch", Appl. Phys. Lett. 112 (2018) 063505

(2) Ilyas, N., Cook, A., Tabor, C. E., Adv. Mater. Interfaces 2017, 4, 1700141.

(3) Wang, D., Lin, Z., Zhou, C., Gao, C. and He, Q. (2019), Liquid Metal Gallium Micromachines Speed Up in Confining Channels. Adv. Intell. Syst., 1: 1900064.

(4) Bilodeau, R. A., Zemlyanov, D. Y., Kramer, R. K., *Adv. Mater. Interfaces* 2017, 4, 1600913.